

Tight factorizations of girth- g -regular graphs

Italo J. Dejter

University of Puerto Rico
Rio Piedras, PR 00936-8377
italo.dejter@gmail.com

Abstract

Girth-regular graphs with equal girth, regular degree and chromatic index are studied for the determination of 1-factorizations with each 1-factor intersecting every girth cycle. Applications to hamiltonian decomposability and to 3-dimensional geometry are given. Applications are suggested for priority assignment and optimization problems.

1 Introduction

Let $3 \leq \kappa \in \mathbb{Z}$. Given a finite graph Γ with girth $g(\Gamma) = \kappa$ we inquire whether assigning κ colors to the edges of Γ *properly* (i.e., no two adjacent edges of equal color in Γ) can be performed so that each κ -cycle of Γ has a bijection from the edges of Γ to the κ colors. Such an inquiry is applicable to managerial situations in which a number of agents must participate in committees around round tables, with κ stools about each table. A roster of κ tasks is handed to each agent at each round table, and such an agent is assigned each of the κ tasks but at pairwise different tables. This can be interpreted as a 2-way (vertex incidence versus girth-cycle membership) problem of sorting the κ colors according to some prioritization hierarchy. Thus, an assignment problem is developed with a range of potential applications in geometry (Section 8), optimization and decision making; see for example [1, 2, 15, 20, 28, 32]. We pass to formalize our ideas.

Let Γ be a finite connected κ -regular simple graph with *chromatic index* $\chi'(\Gamma) = \kappa$. Let $g = g(\Gamma)$ be the girth of Γ . We say that Γ is a *g -tight graph* if $g = g(\Gamma) = \kappa = \chi'(\Gamma)$. In each g -tight graph Γ it makes sense to look for a proper edge-coloring via κ colors, each girth cycle colored via a bijection between the cycle edges and the colors they are assigned, precisely κ colors. We will say that such a coloring is an *edge-girth coloring* of Γ and, in such a case, that Γ is *edge-girth chromatic*, or *egc* for short.

We focus on g -tight κ -regular graphs that are *girth-regular*, a concept whose definition in [22] we adapt as follows. Let Γ be a graph. Let $\{e_1, \dots, e_\kappa\}$ be the set of edges incident in Γ to a vertex v . Let (e_i) be the number of κ -cycles containing an edge e_i for $1 \leq i \leq \kappa$. Assume $(e_1) \geq (e_2) \geq \dots \geq (e_\kappa)$. Let the *signature* of v be the κ -tuple $((e_1), (e_2), \dots, (e_\kappa))$. The graph Γ is said to be *girth-regular* if all its vertices have a common signature. In such a case, the signature of any vertex of Γ is said to be the *signature* of Γ .

In this work, girth-regular graphs that are g -tight will be said to be *girth- g -regular graphs* as well as $((e_1), (e_2), \dots, (e_g))$ -graphs, or $(e_1)(e_2) \cdots (e_g)$ -graphs, if no confusion arises, where $g = \kappa$. In this notation, a prefix

$$a_1^{(1)} a_1^{(2)} \cdots a_1^{(m_1)} a_2^{(1)} a_2^{(2)} \cdots a_2^{(m_2)} \cdots a_t^{(1)} a_t^{(2)} \cdots a_t^{(m_t)}$$

with $a_i^{(j)} = a_{i'}^{(j')}$ iff $i = i'$ may be abbreviated as $a_1^{m_1} a_2^{m_2} \cdots a_t^{m_t}$ where superscripts equal to 1 may be omitted (e.g., 3221 abbreviates to 32^21). So, the prefixes $(e_1)(e_2) \cdots (e_g)$ will include and further be denoted as follows:

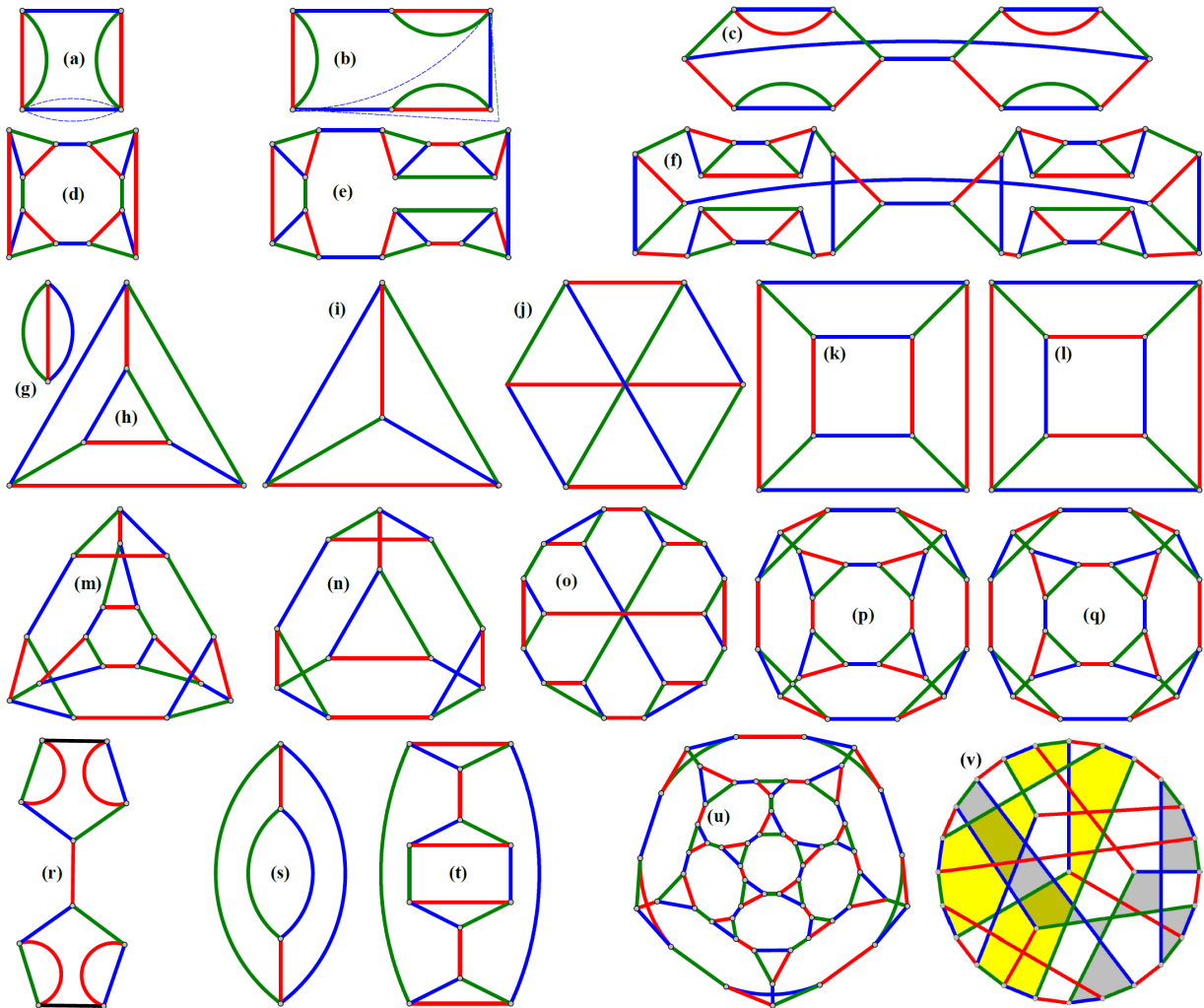


Figure 1: Producing egc $(e_1)(e_2)(e_3)$ -graphs Γ that are triangle-replaced graphs from graphs Γ' . In particular, pairs $(\Gamma)(\Gamma')$ represented here are: (a)(d), (b)(e), (c)(f), (g)(h), (h)(m), (i)(n), (j)(o), (k)(p), (l)(q) and (s)(t). In addition, item (r) is an example of a generalized snark other than the Petersen graph. Items (u) and (v) are related to the dodecahedral graph and to the Coxeter graph, respectively.

- (i) $222 = 2^3$ and $110 = 1^20$ in Section 2, (Theorems 1 and 4);
- (ii) $3333 = 3^4$ $3322 = 3^22^2$ and $2222 = 2^4$ in Section 3, (Theorem 10, via Lemma 9);
- (iii) $4443 = 4^33$ $3221 = 32^21$ and $3111 = 31^3$ in Section 4, (Theorem 21);
- (iv) $1111 = 1^4$ in Section 5, (Theorems 24 and 27, via Lemma 9, or a variation of it);

(v) $44400 = 4^3 0^2 2^3 0^2 8^5$ and $(12)^5$ in Section 6, (Theorems 28, 29, 30 and 31).

Extending this context, girth-regular graphs Γ of regular degree g and girth larger than g will be said to be 0^g -graphs, or *improper* $(e_1)(e_2) \cdots (e_g)$ -graphs.

Edge-girth colorings of $(e_1)(e_2) \cdots (e_g)$ -graphs are equivalent to 1-factorizations [29] such that the cardinality of the intersection of each 1-factor with each girth cycle is 1. These factorizations are said to be *tight*, and the resulting colored girth cycles, are said to be *tightly colored*. Note a Γ with a tight factorization is *egc*. Unions of pairs of 1-factors of such graphs are treated in Section 7 for their hamiltonian decomposability, (Corollary 36). Applications to Möbius-strip compounds and hollow-triangle polylinks are found in Section 8.

2 Egc girth-3-regular graphs

Theorem 1. [22] *There is only one $(e_1)(e_2)(e_3)$ -graph Γ with $(e_1)(e_2)(e_3) = 222 = 2^3$ namely $\Gamma = K_4$. Moreover, $\Gamma = K_4$ is *egc*. All other proper $(e_1)(e_2)(e_3)$ -graphs are 1^20 -graphs, but not necessarily *egc*.*

Proof. For the first sentence in the statement, we refer to item (1) of Theorem 5.1 [22]. To see that $\Gamma = K_4$ is *egc*, we refer to Fig. 1(i), below. \square

Remark 2. In order to determine which 1^20 -graphs are *egc*, let $\Gamma' = (V', E', \phi')$ be a finite undirected loopless cubic multigraph. Let $e \in E'$ with $\phi'(e) = \{u, v\}$ and $u, v \in V'$. Then, e determines two *arcs* (that is, ordered pairs of end-vertices of e) denoted $(e; u, v)$ and $(e; v, u)$ (if the girth $g(\Gamma')$ of Γ' is larger than 2, then Γ' is a simple graph, a particular case of multigraph). The following definition is an adaptation of a case of the definition of generalized truncation in [13]. Let A' denote the set of arcs of Γ' . A *vertex-neighborhood labeling* of Γ' is a function $\rho : A' \rightarrow \{1, 2, 3\}$ such that for each $u \in V'$ the restriction of ρ to the set $A'(u) = \{(e; u, v) \in A' : e \in E'; \phi'(e) = \{u, v\}; v \in V'\}$ of arcs leaving u is a bijection. For our purposes, we require $\rho(e; u, v) = \rho(e; v, u) \forall e \in E'$ with $\phi'(e) = \{u, v\}$ so that each $e \in E'$ is assigned a well-defined color from the color set $\{1, 2, 3\}$. This yields a 1-factorization of Γ' with three 1-factors that we can call E'_1, E'_2, E'_3 for respective color 1, 2, 3, with E' being the disjoint union $E'_1 \cup E'_2 \cup E'_3$. For the sake of examples in Fig. 1, to be presented below, let colors 1, 2 and 3 be taken as red, blue and green, respectively.

Let K_3 be the triangle graph with vertex set $\{v_1, v_2, v_3\}$. The *triangle-replaced* graph $\nabla(\Gamma')$ of Γ' with respect to 4ρ has vertex set

$$\{(e_i; u, v_i) : u \in V'; 1 \leq i \leq 3\}$$

and edge set

$$\{(e_i; u, v_i)(e_j; u, v_j) | v_i v_j \in E(K_3), u \in V'\} \cup \{u, v_{\rho(e; u, w)})(w, v_{\rho(e; w, u)}) | e \in E'; \phi(e) = \{u, w\}\}.$$

Note that $\nabla(\Gamma')$ is a 1^20 -graph. We will refer to the edges of the form $(e_i; u, v_i)(e_j; u, v_j)$ as ∇ -edges or *triangle edges*, and to the edges $(e_i; u, v_i)(e_j; w, v_j)$ $u \neq w$ as Γ' -edges or *non-triangle edges*. Observe that a Γ' -edge is incident only to ∇ -edges and that each vertex of $\nabla(\Gamma')$ is incident to precisely one Γ' -edge. This yields the following.

Observation 3. [13] Let Γ' be a finite undirected cubic multigraph of girth g . Then, for any vertex-neighborhood labeling ρ of Γ' the shortest cycle in the triangle-replaced graph $\nabla(\Gamma')$ containing a Γ' -edge is of length at least $2g$.

We say that Γ' is a *generalized snark* if its chromatic index $\chi'(\Gamma')$ is larger than 3. Two examples of generalized snark are: (i) the Petersen graph and (ii) the multigraph obtained by joining two $(2k + 1)$ -cycles ($k \geq 1$) via an extra-edge (a bridge between the two $(2k + 1)$ -cycles) and adding k parallel edges to each of the two $(2k + 1)$ -cycles so that the resulting multigraph is cubic, see Fig. 1(r) for $k = 5$. The triangle-replaced graph $\Gamma'_1 = \nabla(\Gamma')$ of a generalized snark Γ' will also be said to be a generalized snark. This denomination will also be used for the triangle-replaced graphs $\Gamma'_{i+1} = \nabla(\Gamma'_i)$ of Γ'_i for $i = 1, 2, \dots$ etc. In addition, we will say that Γ' is *snarkless* if it is not a generalized snark. Clearly, K_4 is snarkless.

Vertex-neighborhood labelings ρ for the examples of Γ' below, represented in Fig. 1, have the elements 1, 2 and 3 of $\rho(A')$ interpreted respectively as edge colors red, blue and green. Now, the smallest snarkless multigraphs $\Gamma' \neq K_4$ are:

- (A) the cubic multigraph Γ'_A of two vertices and three edges in Fig. 1(g), with $\nabla(\Gamma'_A)$ being the triangular prism $\text{Prism}(K_3) = K_2 \square K_3$ in Fig. 1(h), where $V(K_2) = \{0, 1\}$ and \square stands for the graph cartesian product [19];
- (B) the cubic multigraph Γ'_B of four vertices resulting as the edge-disjoint union of a 4-cycle and a 2-factor $2K_2$ in Fig. 1(a), with $\nabla(\Gamma'_B)$ in Fig. 1(d).

Given a snarkless Γ' a new snarkless multigraph Γ'' is obtained from Γ' by replacing any edge e with end-vertices say u, v by the submultigraph resulting as the union of a path $P_4 = (u, u', v', v)$ and an extra edge with end-vertices u', v' . For example, Γ' in Fig. 1(g) as Γ'' in Fig. 1(s) and $\nabla(\Gamma'')$ in Fig. 1(t). Using this replacement of an edge e by the said submultigraph, one can transform the submultigraph Γ'_B with the enclosed blue edge e in item (B), above, into a Γ''_B as in Fig. 1(b), with $\nabla(\Gamma''_B)$ in Fig. 1(e); or with the four red and green edges into a Γ'''_B as in Fig. 1(c), with $\nabla(\Gamma'''_B)$ in Fig. 1(f).

The triangle-replaced graphs $\nabla(\Gamma')$ of snarkless $(e_1)(e_2)(e_3)$ -graphs Γ' either proper or improper, with $(e_1)(e_2)(e_3) \in \{2^3, 1^20, 0^3\}$ yield egc 1^20 -graphs, illustrated from:

1. the graph Γ' in Fig. 1(h), namely $\nabla(\Gamma'_A)$ onto the 1^20 -graph Γ in Fig. 1(m),
2. the graph Γ' in Fig. 1(i), namely K_4 onto the 1^20 -graph Γ in Fig. 1(n),
3. the graph Γ' in Fig. 1(j), namely $K_{3,3}$ onto the 1^20 -graph Γ in Fig. 1(o),
4. the graph Γ' in Fig. 1(k), namely the 3-cube graph Q_3 onto the 1^20 -graph Γ in Fig. 1(p).

This raises the observation that non-equivalent 1-factorizations F and F' of an $(e_1)(e_2)(e_3)$ -graph Γ' like in Fig. 1(k) and Fig. 1(l), respectively, for $\Gamma' = Q_3$ result in non-equivalent 1-factorizations $\nabla(F)$ and $\nabla(F')$ of $\Gamma = \nabla(\Gamma')$ represented in this case on $\Gamma = \nabla(\Gamma') = \nabla(Q_3)$ in Fig. 1(p) and Fig 1(q), respectively. This leads to the final assertion in Theorem 4, below.

Fig. 1(u) is the egc 1^20 -graph given by $\nabla(\Gamma')$ for the dodecahedral graph $\text{Dod} = \Gamma'$ in which the union of any two edge-disjoint 1-factors of a 1-factorization of Γ' yields a Hamilton cycle.

In contrast, the Coxeter graph $\text{Cox} = \Gamma'$ in Fig. 1(v) is non-hamiltonian, but the union of any two of its (edge-disjoint) 1-factors is the disjoint union of two 14-cycles, whose apparent interiors are shaded yellow and light gray in the figure. Thus, $\Gamma = \nabla(\Gamma')$ is an egc 1^2_0 -graph.

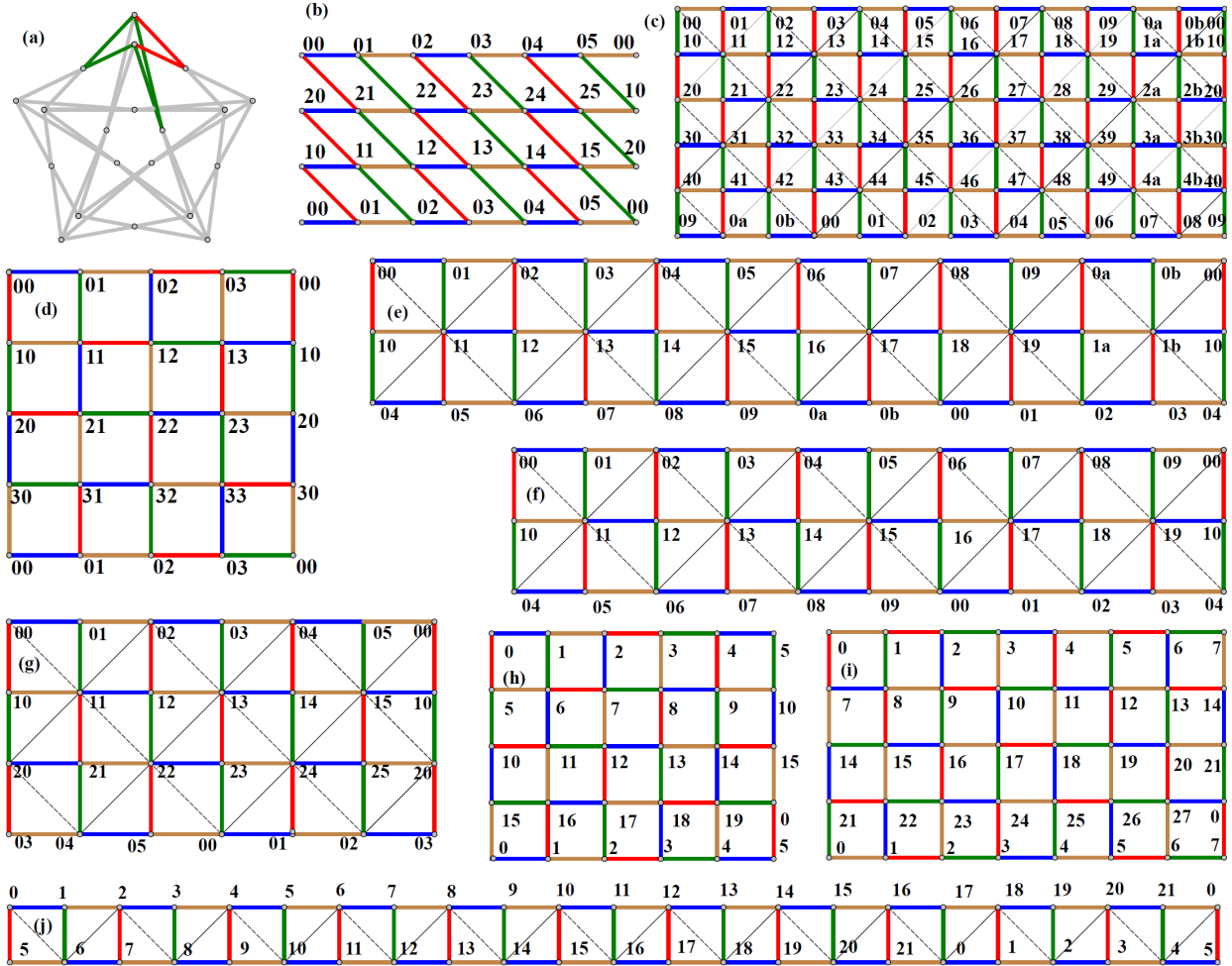


Figure 2: Cutouts of $(e_1)(e_2)(e_3)(e_4)$ -graphs: (a) is the Folkman graph $\mathbb{D}5$; (b) is for a graph embeddable into the Klein bottle; (c) exemplifies Theorem 10 2(e). (d) is for the 4-cube in Theorem 10 1(c); (e) and (f) exemplify Theorem 10 3(b); (g) exemplifies Theorem 10 3(c); (h) and (i) exemplify Theorem 10 2(b); (j) exemplifies Theorem 10 3(a);

Theorem 4. A 1^2_0 -graph Γ is egc if and only if Γ is the triangle-replaced graph of a snark-less Γ' . Moreover, non-equivalent 1-factorizations of such Γ' result in corresponding non-equivalent 1-factorizations of Γ .

Proof. There are two types of edges in a 1^2_0 -graph Γ namely the *triangle edges* (those belonging to some triangle of Γ) and the remaining *non-triangle edges*. Each vertex v of Γ is incident to a unique non-triangle edge e_v and is nonadjacent to a unique edge \bar{e}_v (opposite to v) in the sole triangle T_v of Γ to which v belongs. In any 1-factorization $F = (F_1, \dots, F_g)$ of Γ both e_v and \bar{e}_v belong to the same factor F_i ($i = 1, \dots, g$). Moreover, each edge $e = \{u, v\}$

of Γ (where $e = e_u = e_v$) belongs solely to corresponding triangles T_u and T_v with opposite edges \bar{e}_u and \bar{e}_v . Clearly, $\{e = e_u = e_v, \bar{e}_u, \bar{e}_v\} \subseteq F_i$ with equality given precisely when Γ is the triangular prism in Fig. 1(h).

We will define an inverse operator ∇^{-1} of ∇ that applies to each egc 1^20 -graph Γ . Given one such Γ contracting simultaneously all the triangles T of Γ consists in removing the edges of those T and then identifying the vertices v_1^T, v_2^T, v_3^T of each T into a corresponding single vertex v_T where v_i^T for $i \in \{1, 2, 3\}$ has its unique incident non-triangle edge of Γ with color i . This is done so that whenever two triangles T and T' have respective vertices v_i^T and $v_j^{T'}$ adjacent in Γ ($i, j \in \{1, 2, 3\}$), then $i = j$ and the edge $v_i^T v_j^{T'}$ of Γ is removed and replaced by a new edge $v_T v_{T'}$. The result of these simultaneous triangle contractions is a multigraph $\Gamma' = (V', E', \phi')$ with each $v_T \in V'$ incident to three edges of E' one per each color in $\{1, 2, 3\}$. The ensuing edge coloring in Γ' corresponds to a vertex-neighborhood labeling $\rho : A' \rightarrow \{1, 2, 3\}$ of Γ' from which it follows that Γ is the triangle-replaced graph of Γ' with respect to ρ that is: $\nabla^{-1}(\Gamma) = \Gamma'$. This establishes an identification of Γ and $\nabla(\Gamma')$ so that the triangle-edges of Γ are the ∇ -edges of $\nabla(\Gamma')$ and the non-triangle edges Γ are the Γ' -edges of $\nabla(\Gamma')$. This implies the main assertion of the statement of the theorem. \square

3 Egc girth-4-regular graphs

Remark 5. In this section and in Section 4, we consider $(e_1)(e_2)(e_3)(e_4)$ -graphs Γ with $(e_1)(e_2)(e_3)(e_4) \neq 1111$. Many such graphs are toroidal and obtained from the square tessellation denoted by its Schläfli symbol $\{4, 4\}$. Let T be the group of translations of the plane that preserve such tessellation $\{4, 4\}$. Then, T is isomorphic to $\mathbb{Z} \times \mathbb{Z}$ and acts transitively on the vertices of $\{4, 4\}$. If U is a subgroup of finite index in T then $\mathcal{M} = \{4, 4\}/U$ is a finite map of type $\{4, 4\}$ on the torus, and every such map arises this way ([31], Section 6). A symmetry α of $\{4, 4\}$ acts as a symmetry of \mathcal{M} if and only if α normalizes U . Every such \mathcal{M} has symmetry group $\text{Aut}(\mathcal{M})$ transitive on vertices, horizontal edges and vertical edges. Moreover, for each edge e of \mathcal{M} there is a symmetry that reverses e . The tessellation $\{4, 4\}$ may be considered as a lattice, so it has a *fundamental region* [6, 7]. Such region will be called a *cutout* Φ and be given by a rectangle r squares wide and t squares high, with the left and right edges identified by parallel translation in order to get a toroidal embedding of Γ and the bottom edges identified with the top edges after a shift of s squares to the right, as in Fig. 6 of [31]. A toroidal graph with such a cutout will be denoted:

$$\{4, 4\}_{r,t}^s \tag{1}$$

While the aim of [23, 24, 31] is the study of edge-transitive graphs, we find 1-factorizations of g -tight graphs in graphs $\{4, 4\}_{r,t}^s$ of a more ample nature. Our notation for the vertices of those cutouts will be (i, j) or ij if no confusion arises, where $0 \leq i < r$ and $0 \leq j < t$ as in the examples of tight factorizations in Fig. 2(d), Fig. 2(e), Fig. 2(f), Fig. 2(g), Fig. 2(h), Fig. 2(i) and Fig. 2(j). In particular for $t > 1$ as in Fig. 2(d), Fig. 2(e), Fig. 2(f) and Fig. 2(g), the notation arises from the fact that $\{4, 4\}$ can be considered as the undirected Cayley graph of the direct-sum group $\mathbb{Z} \oplus \mathbb{Z}$ with generator set formed by $(1, 0)$ for horizontal left-to-right arcs and $(0, 1)$ for vertical up-to-down arcs. In case $t = 1$ (Fig. 2(c), Fig. 2(h), Fig. 2(i) and

Fig. 2(j)), we simplify notation by writing i instead of $(i, 0)$ or $i0$. In all of Fig. 2, edge colors are encoded by numbers as follows: 1 for red, 2 for blue, 3 for green and 4 for hazel. (Thin and dashed diagonals of squares are to be used in the proof of Theorem 10).

Remark 6. If a fundamental region Φ of $\{4, 4\}$ as in Remark 5 is identified in reverse on a pair \mathcal{P} of opposite sides, and directly on the other pair, we get a Klein bottle \mathcal{K} [30]. There are egc-graphs that are skeletons of a $\{4, 4\}$ -tessellation of \mathcal{K} for example in Fig. 2(b), whose embedding into \mathcal{K} has corresponding cutout that can be obtained from the one of $\{4, 4\}_{r,t}^s$ above (with $(r, t, s) = (6, 3, 0)$) first by replacing the vertical edges by corresponding square-face diagonals, while keeping the horizontal edges (so the new faces are lozenge rhombi), and second by identifying the horizontal top and bottom borders of the original cutouts, as well as the left and right borders, these with reverse orientations, with the resulting \mathcal{K} -embedding that we will be denoted:

$$[4, 4]_{r,t}^s \quad (2)$$

Then, the example of Fig. 2(b) is in $[4, 4]_{6,3}^0$. If Φ is identified in reverse on both pairs of opposite sides, a projective-planar graph is obtained. This can be ruled out because $\{4, 4\}$ -tessellations only exist on surfaces with Euler characteristic 0.

Remark 7. Let $0 < n \in \mathbb{Z}$. The n -cube graph Q_n has as vertices the n -tuples with entries in \mathbb{Z}_2 and edges only between vertices at unit Hamming distance. In Subsection 3.1, we consider the 4-cube graph $Q_4 = \{4, 4\}_{4,4}^0$. Other $(e_1)(e_2)(e_3)(e_4)$ -graphs with $(e_1)(e_2)(e_3)(e_4) \neq 1111$ and that are not prisms of $(e_1)(e_2)(e_3)$ -graphs are:

- (i) the bipartite complement of the Heawood graph, in Subsection 3.3;
- (ii) the *subdivided double* $\mathbb{D}\Gamma$ [23, 31] of a 4-regular graph Γ is the bipartite graph with vertex set $(V(\Gamma) \times \mathbb{Z}^2) \cup E(\Gamma)$ and an edge between vertices $(v, i) \in V(\Gamma) \times \mathbb{Z}^2$ and $e \in E(\Gamma)$ whenever v is incident to e in Γ ; [23, Lemma 4.2] asserts that if Γ is 4-regular and arc-transitive, then $\mathbb{D}\Gamma$ is 4-regular and semisymmetric; for example, the Folkman graph (Fig. 2(a)) is the subdivided double $\mathbb{D}K_5$ of the complete graph K_5 ;
- (iii) the *circulant graphs*, i.e. the Cayley graphs $C_n(i, j)$ of the cyclic group \mathbb{Z}_n ($n > 6$) with generating sets $\{\pm i, \pm j\}$ where $1 \leq i < j < \frac{n}{2}$ and $\gcd(n, i, j) = 1$; most of these are 2^4 -graphs (assuming n even, otherwise chromatic index is not 4), with additional cycles appearing whenever a congruence $\lambda i \pm (4 - \lambda)j \equiv 0 \pmod{n}$ holds, (e.g., $C_{14}(2, 3)$ is a 2^4 -graph, $C_{12}(2, 3)$ is a $3^2 2^2$ -graph, $C_{10}(1, 3)$ is a 6^4 -graph and $C_8(1, 3) \equiv K_{4,4}$ is a 9^4 -graph); however, such graphs $C_n(i, j)$ can always be seen as toroidal graphs;
- (iv) the *wreath graphs* $W(\underline{n}, 2) = C_n[\overline{K_2}]$ ($n > 4$), i.e. lexicographic products of an n -cycle and the complement $\overline{K_2}$ of K_2 ; these are 5^4 -graphs; ($W(4, 2) \equiv K_{4,4}$ is a 9^4 -graph).

Remark 8. If an $(e_1)(e_2)(e_3)(e_4)$ -graph Γ as in Remark 7 contains a subgraph Γ' guaranteeing that Γ is not an egc-graph, then Γ' is said to be an *egc-obstruction*. A subgraph $\Gamma' \equiv K_{2,3}$ is an egc-obstruction for a girth-4-regular graph Γ since each of the proper edge-colorings of Γ contains a quadrangle of Γ' with only two colors. In Fig. 2(a), one such graph Γ namely

the Folkman graph $\Gamma = \mathbb{D}K_5$ is presented with a subgraph $\Gamma' \equiv K_{2,3}$ formed by a green quadrangle and a red 2-path. $C_{10}(1, 3)$ and $W(6, 2)$ also have obstruction isomorphic to $K_{2,3}$.

The following lemma is a tool for Theorems 9 and 27, and a variation of it, for Theorem 24.

Lemma 9. *A sufficient condition for an $(e_1)(e_2)(e_3)(e_4)$ -graph Γ with $(e_i) < 3$ ($i = 1, 2, 3, 4$) to be egc is existence of 2-factorization $\{F_1, F_2\}$ of Γ such that each 2-factor F_i ($i = 1, 2$):*

1. *is the disjoint union of even-length cycles; and*
2. *has an even-length cycle $D(C)$ as in item 1, for each 4-cycle C of Γ sharing with C exactly two consecutive edges.*

Proof. A 1-factorization of F_1 via colors 1 and 2 and a 1-factorization of F_2 via colors 3 and 4 exist and form a tight 1-factorization of Γ . \square

Theorem 10. *The following 3^4 -, $3^2 2^2$ - and 2^4 -graphs exist, and are egc or not, as indicated, where notations (1) and (2) are used:*

1. 3^4 -graphs comprising the:
 - (a) *bipartite complement of the Heawood graph, which is not egc, (Subsection 3.3);*
 - (b) *4-regular subdivided doubles $\mathbb{D}\Gamma$ of 4-regular graphs Γ which are not egc;*
 - (c) *4-cube graph $Q_4 = \{4, 4\}_{4,4}^0$ which is egc in two different, orthogonally related ways, (Subsections 3.1-3.2, Remark 11; an initial example is in Fig. 2(d));*
2. $2^2 3^2$ -graphs (assuming $0 < t \leq r$ and $0 \leq s < r$), comprising:
 - (a) $\{4, 4\}_{2\ell, 4}^0$: *egc $\Leftrightarrow \ell \in (3, \infty) \cap 2\mathbb{Z}$; (concatenating copies of $\{4, 4\}_{4,4}^0$ in Fig. 2(d));*
 - (b) $\{4, 4\}_{4s, 1}^s$: *egc $\Leftrightarrow s \in (4, \infty) \cap \mathbb{Z} \setminus 2\mathbb{Z}$; (Fig. 2(h-i), for $r_t^s = 20_1^5, 28_1^7$);*
3. 2^4 -graphs (assuming $0 < t \leq r$ and $0 \leq s < r$) comprising:
 - (a) $\{4, 4\}_{r, 1}^s$: *egc $\Leftrightarrow r \in 2\mathbb{Z} \setminus 4\mathbb{Z}$ $s \in \mathbb{Z} \setminus (2\mathbb{Z} \cup 1)$ and $r \neq 3s + 1$; (Fig. 2(j), $r_t^s = 22_1^5$);*
 - (b) $\{4, 4\}_{r, 2}^s$: *egc $\Leftrightarrow r \in [10, \infty) \cap 2\mathbb{Z}$ and $s \in [4, r-4] \cap 2\mathbb{Z}$; (Fig. 2(e-f), $r_t^s = 12_2^4, 10_2^4$);*
 - (c) $\{4, 4\}_{r, 3}^s$: *egc $\Leftrightarrow r \in [6, \infty) \cap 2\mathbb{Z}$ and $s = [3, r-3] \setminus 2\mathbb{Z}$; (Fig. 2(g), $r_t^s = 6_3^3$);*
 - (d) $\{4, 4\}_{r, 4}^s$: *egc $\Leftrightarrow 4 \leq r \in 2\mathbb{Z}$ and $0 < s \in 2\mathbb{Z}$; (color pattern as in Fig. 2(e-g), (j));*
 - (e) $\{4, 4\}_{r, t}^s$ $t \in [4, \infty)$: *egc $\Leftrightarrow r \in 2\mathbb{Z}$ and $t + s \in 2\mathbb{Z}$; (color pattern as in Fig. 2(c));*
 - (f) $[4, 4]_{r, t}^0$: *egc $\Leftrightarrow r \in [6, \infty) \cap 2\mathbb{Z}$ and $t \in [3, \infty) \cap \mathbb{Z} \setminus 2\mathbb{Z}$; (Fig. 2(b), $r_t^s = 6_3^0, 8_3^0$).*

A cycle of a graph Γ as in Remarks 5-6 is said to be *1-zigzagging* if it is formed by alternate horizontal and non-horizontal (i.e., all vertical or all 45°-tilted) edges. A 2-factor of Γ is said to be *1-zigzagging* if its composing cycles are 1-zigzagging. A 2-factorization of Γ is said to be *1-zigzagging* if its composing 2-factors are 1-zigzagging.

Proof. We pass to analyze the different items composing the statement of Theorem 10.

Items 1 and 2: Item 1(a) is proved in Subsection 3.3. The graphs of item 1(b) have egc-obstructions (see Remark 8) formed by three edge-disjoint paths of length 2 between two nonadjacent vertices, e.g., $\mathbb{D}K_5$ in Fig. 2(a), with egc-obstruction formed by four green edges and two red edges. Items 1(c) and 2(b) are proved in Subsection 3.2, Remark 11; (see also Fig. 2(d)). Item 2(a) is proved by concatenating copies of $\{4, 4\}_{4,4}^0$ as in Fig. 2(d).

Item 3: Lemma 9 applies to each Γ as in Remarks 5-6 via the 1-zigzagging 2-factorization (12)(34) which contains its 2-factors having exactly two consecutive edges in common with each 4-cycle, as shown in Fig. 2(e,f,g,j,b,c). In items 3(a-f), the non-egc cases indicated via “ \Leftrightarrow ” include those not satisfying the sufficient condition of Lemma 9, because such condition becomes also necessary for each Γ arising from a toroidal or Klein-bottle cutout as in Remarks 5–6. Moreover, all the 1-zigzagging cycles in Γ have even length and share two consecutive edges with each 4-cycle precisely where indicated via “ \Leftrightarrow ” in items 3(a-f). Furthermore, in Fig. 2(e,f,g,j), the thin diagonals separate those pairs of consecutive edges (for the 2-factorization (12)(34)), while the dashed ones do the same for the 2-factorization (14)(23). In addition, note the exclusion in item 3(a) of the cases $\{4, 4\}_{6,1}^1$ and those for which $r = 3s + 1$ and in item 3(c) the case $\{4, 4\}_{6,3}^1$. In item 3(b), note the lower bound for r due to $\{4, 4\}_{8,2}^4$ being a $3^2 2^2$ -graph but not egc. For item 3(e), the case $s = 0$ is covered in item 2(a).

For the cases of Klein-bottle graphs in item 3(f), there are two different color patterns, the first one, exemplified in Fig. 2(b), valid for $6 \leq r \in 2\mathbb{Z}$ and the second one further restricted to having $r \in 4\mathbb{Z}$ with more than two colors on each horizontal line. Note the exclusion of the cases $[4, 4]_{4,t}^0$ ($3 < t \in \mathbb{Z} \setminus 2\mathbb{Z}$), for they are not girth-regular. \square

The egc-cases of Theorem 10 item 3 are exemplified respectively in Fig. 2(e,f,g,j,b,c), characterized by having cycles with blue-hazel horizontal edges and cycles with red-green non-horizontal edges. However, transposing the two colors in 1-zigzagging cycles of 2-factors in 2-factorizations (12)(34) (13)(24) or (14)(23) yield tight factorizations with horizontal cycles colored with more than 2 colors.

3.1 The 4-cube as a twice-egc girth-4-regular graph

Consider the three mutually orthogonal Latin squares of order 4, or MOLS(4) [5] contained as the second, third and fourth rows in the following compound matrix:

$$\begin{array}{c|cccc}
 & 1 & 2 & 4 & 7 \\
 \hline
 0 & 111 & 222 & 333 & 444 \\
 3 & 243 & 134 & 421 & 312 \\
 5 & 324 & 413 & 142 & 231 \\
 6 & 432 & 341 & 214 & 123
 \end{array} \tag{3}$$

where for us row and column headings will stand for the following 4-tuples:

$$\begin{aligned}
 0 &= 0000, & 1 &= 1000, & 2 &= 0100, & 3 &= 1100, & 4 &= 0010, & 5 &= 1010, & 6 &= 0110, & 7 &= 1110, \\
 0' &= 0001, & 1' &= 1001, & 2' &= 0101, & 3' &= 1101, & 4' &= 0011, & 5' &= 1011, & 6' &= 0111, & 7' &= 1111.
 \end{aligned} \tag{4}$$

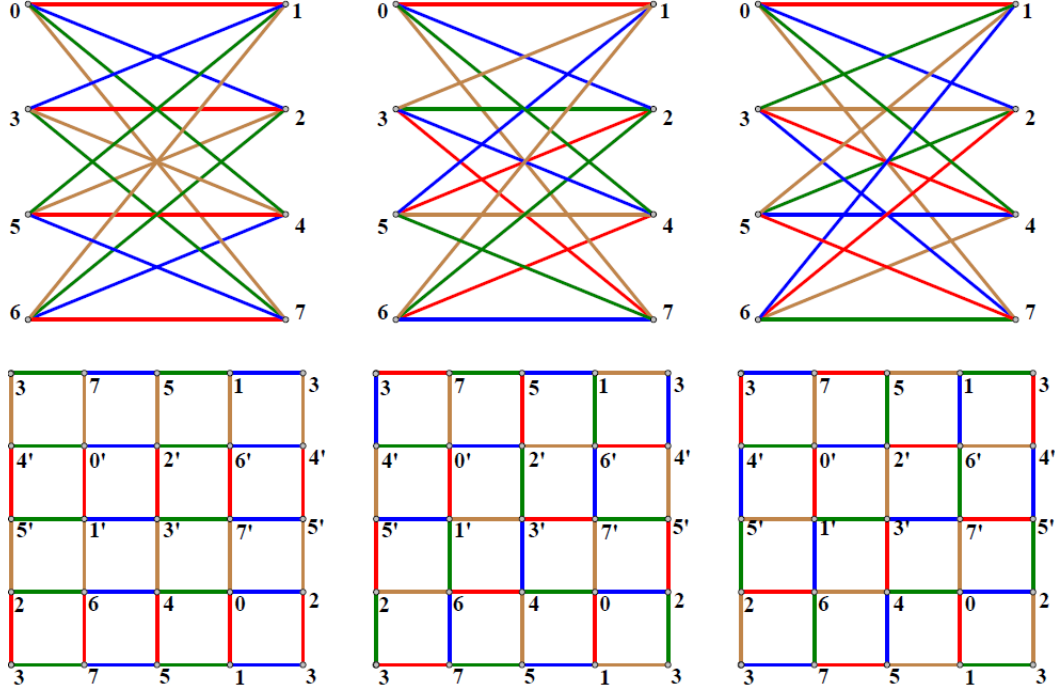


Figure 3: On top of the figure there are represented three 1-factorizations of $K_{4,4}$. Below them, corresponding toroidal cutouts of Q_4 are drawn, with 0-, 1- and 2-color 4-cycles.

Based on display (3), the top of Fig. 3 contains three copies of $K_{4,4}$ properly colored in a mutually-orthogonal way, where colors are numbered as established in Remark 5. Letting $\phi : Q_4 \rightarrow K_{4,4}$ be the canonical projection map of Q_4 seen as a double covering of $K_{4,4}$ obtained by identifying the pairs of antipodal vertices of $Q_4 = \{4, 4\}_{4,4}^0$ these vertices denoted as in display (4), note that in the bottom of Fig. 3 corresponding copies of the colored inverse images $\phi^{-1}(K_{4,4})$ of the three mentioned copies of $K_{4,4}$ are depicted. The leftmost copy of Q_4 in Fig. 3 has color i attributed precisely to those edges parallel to the i^{th} coordinate direction, for $i = 1, 2, 3, 4$. This constitutes a 1-factorization $F_0 = \{F_0^1, F_0^2, F_0^3, F_0^4\}$ of Q_4 . On the other hand, the center and rightmost copies of Q_4 in the figure determine 1-factorizations F_1 and F_2 of Q_4 for which each girth cycle of Q_4 intersects every composing 1-factor F_i^j of F_i where $i = 1, 2$ and $j = 1$ (red), 2 (blue), 3 (green), 4 (hazel).

For each edge e of Q_4 we say that e has i -color $j \in \{1, 2, 3, 4\}$ if $e \in F_i^j$. Then, each 4-cycle of Q_4 has opposite edges with a common 0-color in $\{1, 2, 3, 4\}$ with a total of two (nonadjacent) 0-colors in $\{1, 2, 3, 4\}$ per 4-cycle, say 0-colors $\ell_1, \ell_2 \in \{1, 2, 3, 4\}$ with $\ell_1 \neq \ell_2$ so one such 4-cycle can be expressed as $(\ell_1, \ell_2, \ell_1, \ell_2)$. On the other hand, the 4-cycles of Q_4 use all four i -colors 1,2,3,4, once each, for $i = 1, 2$.

There are twenty-four 4-cycles in Q_4 six of each of the 0-color 4-cycles expressed in the first two columns of the following array, with two complementary 0-color 4-cycles per row. On the other hand, the third and fourth columns here contain respectively the 1-color and 2-color 4-cycles corresponding to the 0-color 4-cycles in the first two columns:

(1212)	(3434)	(1234)	(1243)
(1313)	(2424)	(1324)	(1342)
(1414)	(2323)	(1423)	(1432)

(5)

3.2 Toroidal representation tables

Remark 11. The triple array in Table 1 presents F_i ($i = 0, 1, 2$) in schematic representations of $Q_4 = \{4, 4\}_{4,4}^0$ where \circ stands for a vertex of Q_4 and \square stands for an i -color 4-cycle. This table guarantees Theorem 10 item 3(c) via the last two columns of color quadruples in display (5), because the four colors are employed on the edges of each 4-cycle:

\circ 3 \circ 2 \circ 3 \circ 2 \circ	\circ 1 \circ 3 \circ 2 \circ 4 \circ	\circ 2 \circ 1 \circ 4 \circ 3 \circ
4 \square 4 \square 4 \square 4 \square 4	2 \square 4 \square 1 \square 3 \square 2	1 \square 4 \square 3 \square 2 \square 1
\circ 3 \circ 2 \circ 3 \circ 2 \circ	\circ 3 \circ 2 \circ 4 \circ 1 \circ	\circ 3 \circ 2 \circ 1 \circ 4 \circ
1 \square 1 \square 1 \square 1 \square 1	4 \square 1 \square 3 \square 2 \square 4	2 \square 1 \square 4 \square 3 \square 2
\circ 3 \circ 2 \circ 3 \circ 2 \circ	\circ 2 \circ 4 \circ 1 \circ 3 \circ	\circ 4 \circ 3 \circ 2 \circ 1 \circ
4 \square 1 \square 4 \square 1 \square 4	1 \square 3 \square 2 \square 4 \square 1	3 \square 2 \square 1 \square 4 \square 3
\circ 3 \circ 2 \circ 3 \circ 2 \circ	\circ 4 \circ 1 \circ 3 \circ 2 \circ	\circ 1 \circ 4 \circ 3 \circ 2 \circ
1 \square 1 \square 1 \square 1 \square 1	3 \square 2 \square 4 \square 1 \square 3	4 \square 3 \square 2 \square 1 \square 4
\circ 3 \circ 2 \circ 3 \circ 2 \circ	\circ 1 \circ 3 \circ 2 \circ 4 \circ	\circ 2 \circ 1 \circ 4 \circ 3 \circ

Table 1: Representations of F_i ($i = 0, 1, 2$) corresponding to the three representations of Fig. 3, where the toroidal cutouts are represented with vertices given with symbols \circ and 4-cycles given with symbols \square . The edge colors 1, 2, 3, 4 replace the lines between the vertices \circ .

- (a) either as horizontal or vertical color quadruples (as in display 5) alternated with the symbols \circ that represent the vertices of Q_4 ;
- (b) or as quadruples around the symbols \square representing the other 4-cycles.

By associating the oriented quadruple $(1,3,2,4)$ (resp. $(3,4,1,2)$) of successive edge colors on the left-to-right and the downward (resp. the right-to-left and the downward) straight paths in F_1 (resp. F_2), situations that we indicate by “ $\searrow (1, 3, 2, 4)$ ” (resp. “ $\swarrow (3, 4, 1, 2)$ ”), a complete invariant for F_1 (resp. F_2) is obtained that we denote by combining between square brackets the just presented notations:

$$[a_{\swarrow 12,34}, b_{\searrow 13,24}, \searrow (1, 3, 2, 4)], \text{ (resp. } [a_{\searrow 13,24}, b_{\swarrow 12,34}, \swarrow (3, 4, 1, 2))].$$

This invariant distinguishes F_1 and F_2 from each other and is generalized for the toroidal graphs in Theorem 10, as we will see below in this subsection.

Table 1 is also presented to establish similar patterns, like in Table 2, allowing in a likewise manner to guarantee Theorem 10 item 2(b). We say that

00	2	01	4	02	1	03	3	04	2	05	00	2	01	1	02	3	03	4	04	2	05	1	06	3	07
1	□	3	□	2	□	4	□	1	□	3	1	□	3	□	4	□	2	□	1	□	3	□	4	□	2
05	4	06	1	07	3	08	2	09	4	10	07	4	08	2	09	1	10	3	11	4	12	2	13	1	14
3	□	2	□	4	□	1	□	3	□	2	2	□	1	□	3	□	4	□	2	□	1	□	3	□	4
10	1	11	3	12	2	13	4	14	1	15	14	3	15	4	16	2	17	1	18	3	19	4	20	2	21
2	□	4	□	1	□	3	□	2	□	4	4	□	2	□	1	□	3	□	4	□	2	□	1	□	3
15	3	16	2	17	4	18	1	19	3	00	21	1	22	3	23	4	24	2	25	1	26	3	27	4	00
4	□	1	□	2	□	3	□	4	□	1	3	□	4	□	2	□	1	□	3	□	4	□	2	□	1
00	2	01	4	02	1	03	3	04	2	05	00	2	01	1	02	3	03	4	04	2	05	1	06	3	07

Table 2: In this table, instead of \circ standing for each vertex, we set the vertex notation of $\{4, 4\}_{20,1}^5$ in Fig. 2(h) and $\{4, 4\}_{28,1}^5$ in Fig. 2(i). Here the four colors are indicated as in Fig. 2(d–j) and Subsection 3.1. To distinguish these two cases, note that the 4-cycles of $\{4, 4\}_{20,1}^5$ (resp. $\{4, 4\}_{28,1}^5$) have the 2-factors by color pairs $\{1, 2\}$ and $\{3, 4\}$ descending in zigzag from right to left (resp. left to right), by alternate vector displacements $(-1, 0)$ (resp. $(1, 0)$) for colors 1 and 3, and $(0, -1)$ for colors 2 and 4.

1. F_1 has $a_{\swarrow_{12,34}}$ -zigzags if any 1-zigzagging path obtained by walking left, down, left, down and so on, alternates either colors 1 and 2, or colors 3 and 4;
2. F_1 has $b_{\searrow_{13,24}}$ -zigzags if any 2-zigzagging path obtained by walking right, right, down, down and so on, alternates either colors 1 and 3, or colors 2 and 4;
3. F_2 has $a_{\searrow_{13,24}}$ -zigzags if any 2-zigzagging path obtained by walking left, left, down, down and so on, either alternates colors 1 and 2, or colors 3 and 4;
4. F_2 has $b_{\swarrow_{12,34}}$ -zigzags if any 1-zigzagging path obtained by walking right, down, right, down and so on, either alternates colors 1 and 3, or colors 2 and 4.

A representation as in Table 1 may be used for the graphs in items 1(b) and 2 of Theorem 10. For example, the cases $(r, t, s) = (20, 1, 5)$ and $(r, t, s) = (28, 1, 5)$ in Fig. 2(h–i) are representable as in Table 2, where, instead of \circ standing for each vertex, we set the vertex notation of Fig. 2(h–i). Here the four colors are indicated as in Fig. 2(d–j) and Subsection 3.1. To distinguish these two cases in Table 2, note that the 4-cycles of $\{4, 4\}_{20,1}^5$ (resp. $\{4, 4\}_{28,1}^5$) have the 2-factors by color pairs $\{1, 2\}$ and $\{3, 4\}$ descending in zigzag from right to left (resp. left to right), by alternate vector displacements $(-1, 0)$ (resp. $(1, 0)$) for colors 1 and 3, and $(0, -1)$ for colors 2 and 4. Generalizing and using the invariant notation of Remark 11, we can say that the egc graphs in item 2(b) of Theorem 10 are as follows:

1. $\{4, 4\}_{6x+2,1}^5$ for $x > 2$ has invariant $[a_{\swarrow_{12,34}}, b_{\searrow_{13,24}}, \searrow (2, 4, 1, 3)]$;
2. $\{4, 4\}_{6x+4,1}^5$ for $x > 2$ has invariant $[a_{\swarrow_{13,24}}, b_{\searrow_{12,34}}, \swarrow (2, 4, 3, 1)]$.

As in Remark 11, we have here a distinguished oriented slanted arrow triple: either $[\swarrow, \searrow, \searrow]$ or $[\searrow, \swarrow, \swarrow]$. The graphs in item 2 of Theorem 10 admit both invariants.

3.3 The bipartite complement of the Heawood graph

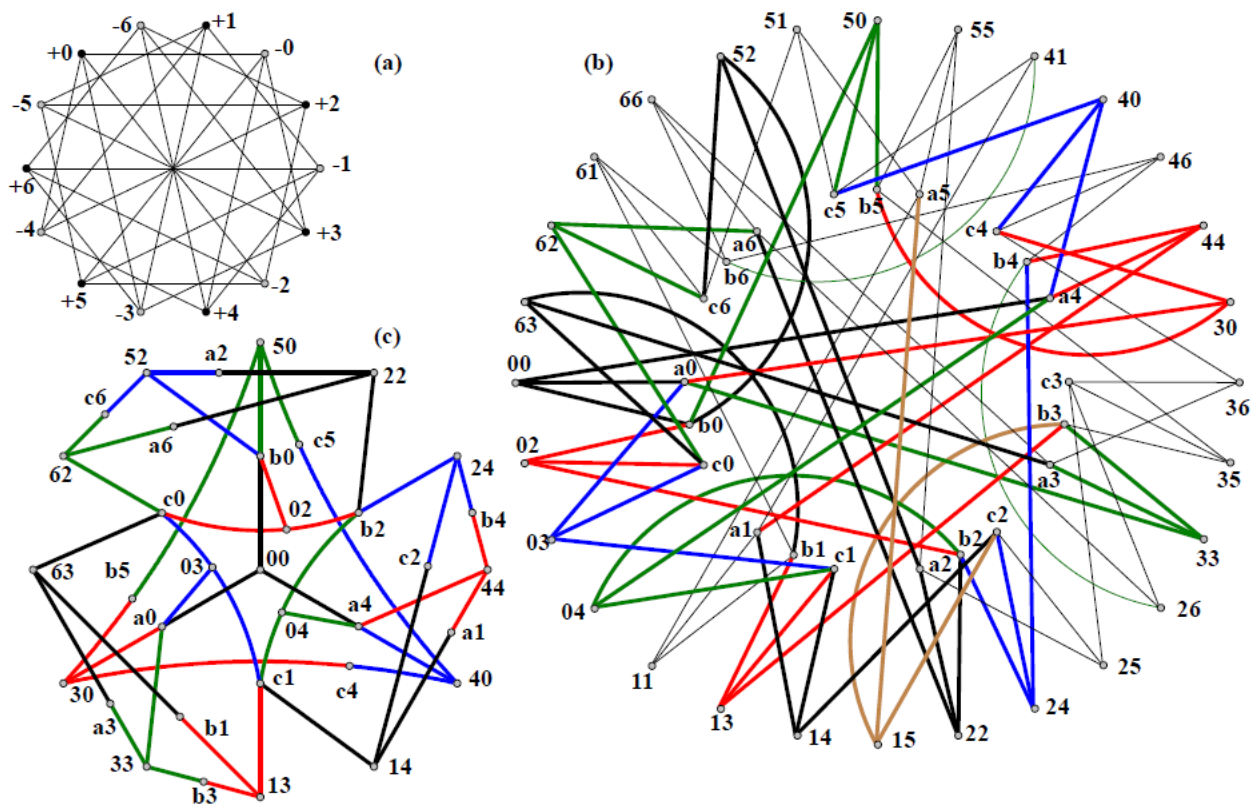


Figure 4: The bipartite complement H of the Heawood-graph, with vertex set $V(H) = \{ij; i \in \{+, -\} j \in \mathbb{Z}_7\}$ is depicted on the upper left, (a), of the figure; its edges $\{+j, -j\}$ $\{+j, -(j+2)\}$ $\{+j, -(j+3)\}$ and $\{+j, -(j+4)\}$ for $j \in \mathbb{Z}_7$ are denoted jj $j(j+2)$ $j(j+3)$ and $j(j+4)$ respectively, where addition is taken (mod 7). Its associated graph $GA(H)$ is depicted on the right, (b), of the figure. This forces the coloring of the subgraph of $GA(H)$ in the lower left, (c), of the figure.

The bipartite complement H of the Heawood-graph, with vertex set $V(H) = \{ij; i \in \{+, -\} j \in \mathbb{Z}_7\}$ is depicted on the upper left of Fig. 4; its edges

$$\{+j, -j\}, \{+j, -(j+2)\}, \{+j, -(j+3)\} \text{ and } \{+j, -(j+4)\},$$

for $j \in \mathbb{Z}_7$ will be denoted

$$jj, j(j+2), j(j+3) \text{ and } j(j+4), \text{ respectively,}$$

where addition is taken (mod 7). This yields the twenty-eight edges of H as arcs from $+$ to $-$ vertices. They form twenty-one 4-cycles a_i, b_i, c_i ($i \in \mathbb{Z}_7$) expressed, by omitting the signs \pm as in Table 3.

This way,

$$jj = a_j \cap a_{j+4} \cap b_j, j(j+2) = b_j \cap b_{j+2} \cap c_j, j(j+3) = a_j \cap c_j \cap c_{j+1} \text{ and } j(j+4) = a_{j+4} \cap b_{j+2} \cap c_{j+1},$$

$a_0 = (00, 30, 33, 03),$	$b_0 = (00, 50, 52, 02),$	$c_0 = (02, 62, 63, 03),$
$a_1 = (11, 41, 44, 14),$	$b_1 = (11, 61, 63, 13),$	$c_1 = (13, 03, 04, 14),$
$a_2 = (22, 52, 55, 25),$	$b_2 = (22, 02, 04, 24),$	$c_2 = (24, 14, 15, 25),$
$a_3 = (33, 63, 66, 36),$	$b_3 = (33, 13, 15, 35),$	$c_3 = (35, 25, 26, 36),$
$a_4 = (44, 04, 00, 40),$	$b_4 = (44, 24, 26, 46),$	$c_4 = (46, 36, 30, 40),$
$a_5 = (55, 15, 11, 51),$	$b_5 = (55, 35, 30, 50),$	$c_5 = (50, 40, 41, 51),$
$a_6 = (66, 26, 22, 62),$	$b_6 = (66, 46, 41, 61),$	$c_6 = (61, 51, 52, 62).$

Table 3: The twenty-one 4-cycles a_i, b_i, c_i of H ($i \in \mathbb{Z}_7$).

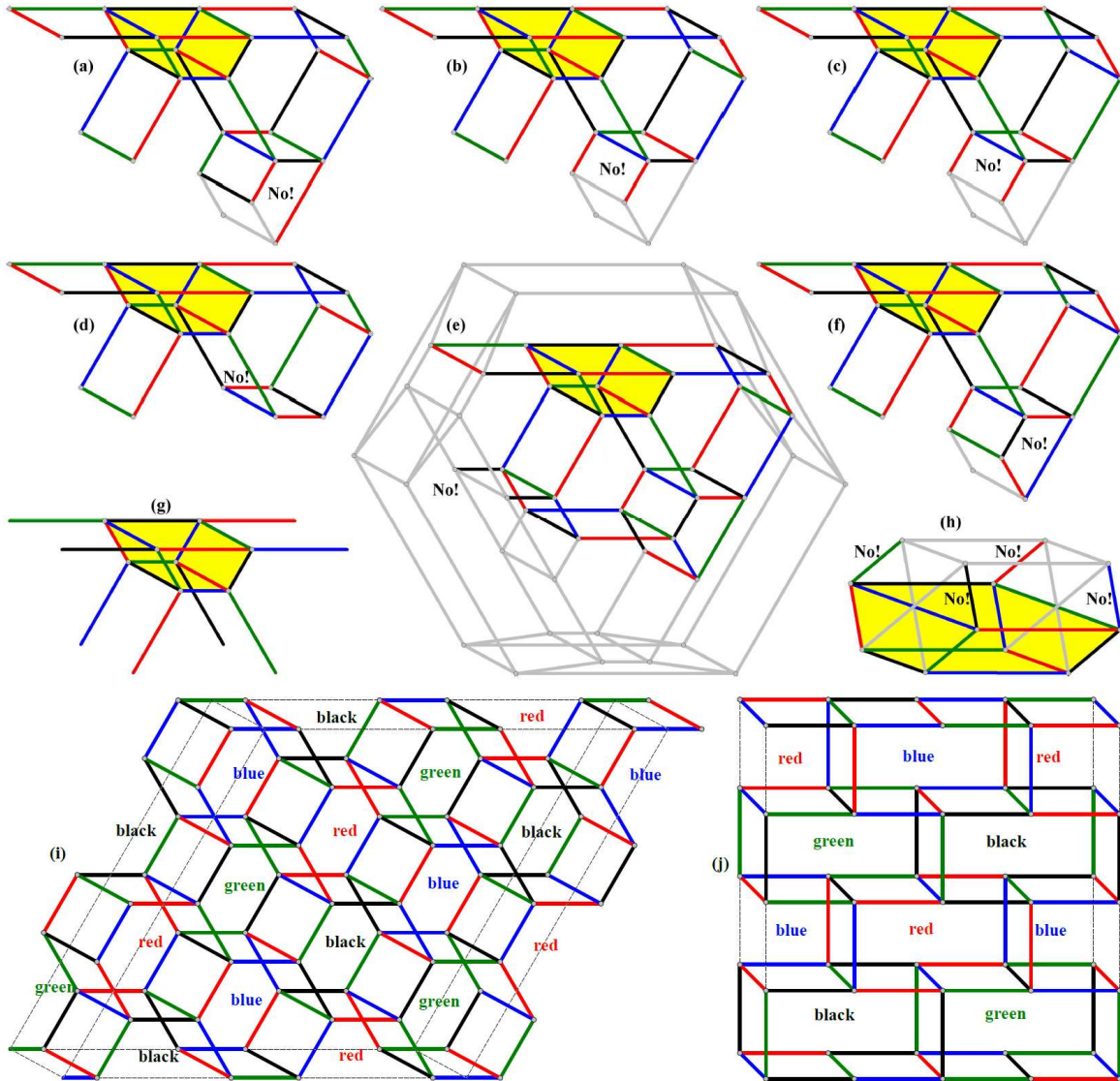


Figure 5: Cases of prisms of: truncated octahedron 32^21 in (a)–(g), $K_{3,3} 4^3 3$ in (h), $ST_4 31^3$ in (i) and a 16-vertex graph 31^3 in (j), where the first two cases are shown not to be egc by arguments presented in the text, and the last two cases are explicitly shown to be egc.

$\forall j \in \mathbb{Z}_7$. We show there is no proper edge coloring of H that is tight on every 4-cycle. To prove this, we recur to the bipartite graph $\text{GA}(H)$ whose parts V_1 and V_2 are respectively the twenty-eight edges and twenty-one 4-cycles of H with adjacency between an edge ij of H and a 4-cycle C of H whenever C passes through ij .

$\text{GA}(H)$ is represented in Fig. 4(b) with a_i written as ai ($i = 1, 2, 3$). A tight factorization of H would be equivalent to a 4-coloring of $\text{GA}(H)$ that is monochromatic on each vertex of V_1 but covering the four colors at the edges incident to each vertex of V_2 . We begin by coloring the edges incident to vertices 00, 02, 03, 04 respectively with colors black, red, blue and green. This forces the coloring of the subgraph of $\text{GA}(H)$ in the lower left of Fig. 4. By transferring this coloring to the representation of $\text{GA}(H)$ on the right of Fig. 4, as shown, it is verified that vertex 15 on the bottom of the representation does not admit properly any of the four used colors.

4 Prisms of types 4443, 3221 and 3221

Given a graph Γ' the prism graph $\text{Prism}(\Gamma')$ of Γ' is the graph cartesian product $K_2 \square \Gamma'$. The cases of $(e_1)(e_2)(e_3)(e_4)$ -graphs with $(e_1)(e_2)(e_3)(e_4) \neq 1^4$ apart from those treated in Section 3, are the prisms $\Gamma = \text{Prism}(\Gamma')$ of $(e_1)(e_2)(e_3)$ -graphs Γ' . It is easy to see that there is no egc graph Γ if $g(\Gamma')$ is odd.

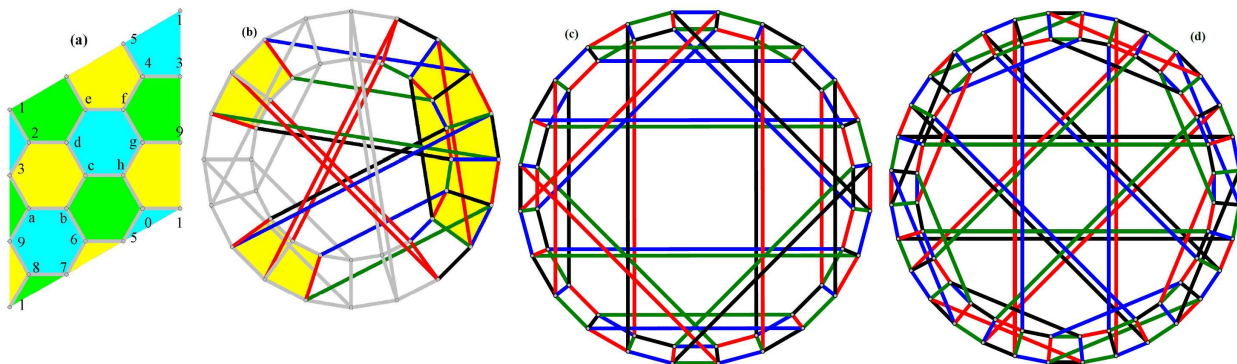


Figure 6: A Pappus-graph cutout and the Desargues, Nauru and Dyck graph prisms.

Conjecture 12. Graphs Γ with signatures 32^21 and 4^33 are not egc.

Example 13. Conjecture 12 is sustained by the exhaustive partial colorings of the prisms of the 24-vertex truncated octahedral graph [11, pp. 79–86] in Fig. 5(a–g) and of the 6-vertex Thomsen graph $K_{3,3}$ [10] in Fig. 5(h), which are respectively a 32^21 -graph and a 4^33 -graph, with the incidental obstructions indicated by a notification "No!" in each case. Such exhaustive partial colorings can be found similarly for example in the 120-vertex truncated-icosidodecahedral graph [11, pp. 97–99].

Remark 14. A 31^3 -graph $\Gamma = K_2 \square \Gamma'$ where Γ' is a toroidal quotient graph of the hexagonal tessellation [6, 7] (i.e. the tiling of the plane with Schläfli symbol $\{6, 3\}$), may be an egc 31^3 -graph. This is exemplified in Fig. 5(i–j), namely for the prisms of the 24-vertex star graph

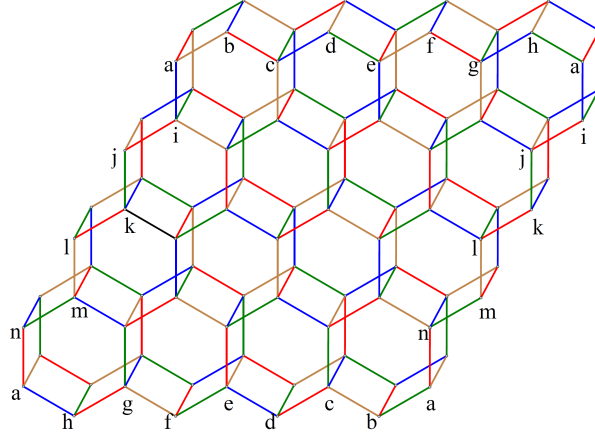


Figure 7: An edge-girth coloring of the prism of $\{6, 3\}_{|4,4|}$ on the Klein bottle. Note that the colorings of the hexagonal prisms in which one color appears six times only occur in the first row, and no edge-girth coloring of this graph is possible if only such colorings are used.

ST_4 (with twelve girth 6-cycles) [12] and a 16-vertex graph (with just eight girth 6-cycles). But Γ' cannot be the Pappus graph. Let us see why. A cutout in this case, as in Fig. 6(a) (with octodecimal vertex notation and proper face coloring) contains nine hexagonal tiles. In order to use the specified coloring to guarantee the existence of an egc-graph, the “period” employed when moving from any particular vertex v_R of a cutout R in any of the three directions perpendicular to the edges of the tessellation – i.e., the number of tiles met until a similar vertex $v_{R'}$ in a cutout R' adjacent to R is reached – must be even, but 9 is odd, leading to a contradiction.

Remark 15. In the setting of Remark 14, by considering the junction of three hexagonal prisms P_1, P_2, P_3 it is seen that in any such P_i ($i = 1, 2, 3$), two edges not belonging to a hexagon can only be of the same color if their endpoints are antipodal in the two hexagons of P_i . Up to automorphism and permutation of colors, this allows for two distinct colorings of the hexagonal prisms:

1. the one as in both instances of Fig. 5(i-j) (with one color appearing on six edges and the remaining four colors appearing each on four edges), and
2. one with two colors appearing each on five edges and the other two colors appearing each on four edges.

See Fig. 7, explained in Example 18, below. Computational evidence has been obtained that gives support to the following conjectures.

Conjecture 16. The condition of even periods in Remark 14 is sufficient for the case of prisms of hexagonal tessellations of the torus.

Conjecture 17. The prisms of the hexagonal tessellations of the Klein bottle [30] are egc if the cutout contains $m \times n$ tiles, with m and n even, and having both types of colorings of the hexagonal prism as in Remark 15.

Example 18. Conjecture 17 is sustained by the prism cutout in Fig. 7, showing an edge-girth coloring of the prism of $\{6, 3\}_{|4;4|}$ [30] on the Klein bottle. Note that the colorings of the hexagonal prisms in which one color appears six times only occur in the first row, and no edge-girth coloring of this graph is possible if only such colorings are used.

Example 19. In Fig. 6(b), the prism of the Desargues graph on twenty vertices is shown non-egc via obstructions by pairs of forced “long” parallel red edges. However, in Fig. 6(c–d) the Nauru and Dyck graphs on twenty-four and thirty-two vertices, respectively, are shown to have their prisms as egc graphs by means of corresponding tight factorizations.

Example 20. For the case $g(\Gamma') = 8$ let us consider Γ' to be the Tutte 8-cage on 30 vertices. Fig. 8(a–c) shows why its 31^3 -graph prism is not egc, with five 8-cycle prisms $K_2 \square C_8$ in Γ (presented cyclically mod 5), each of whose vertices should have its four incident edges colored differently. In fact, Fig. 8(a–c) presents exhaustively without loss of generality partial edge-colorings in Γ with copies of $K_2 \square C_8$ edge-colored accordingly and notification “No!” if an obstruction to edge-coloring continuation appears.

$\bar{3}$	$\bar{3}$	4	1	2	3	$\bar{4}$	$\bar{3}$	4	2	1	3	$\bar{4}$	$\bar{4}$	3	2	1	4	$\bar{3}$	$\bar{4}$	3	1	2	4
$\circ 4$	$\circ 1$	$\circ 2$	$\circ 3$	$\circ 4$	$\circ 1$	$\circ 2$	$\circ 1$	$\circ 3$	$\circ 4$	$\circ 2$	$\circ 1$	$\circ 3$	$\circ 2$	$\circ 1$	$\circ 4$	$\circ 3$	$\circ 2$	$\circ 1$	$\circ 2$	$\circ 4$	$\circ 3$	$\circ 1$	$\circ 2$
$\square 1$	$\square 2$	$\square 3$	$\square 4$	$\square 1$	$\square 2$	$\square 3$	$\square 4$	$\square 2$	$\square 1$	$\square 3$	$\square 4$	$\square 2$	$\square 1$	$\square 4$	$\square 3$	$\square 2$	$\square 1$	$\square 4$	$\square 3$	$\square 1$	$\square 2$	$\square 4$	$\square 3$
$\circ 3$	$\circ 4$	$\circ 1$	$\circ 2$	$\circ 3$	$\circ 4$	$\circ 1$	$\circ 3$	$\circ 4$	$\circ 2$	$\circ 1$	$\circ 3$	$\circ 4$	$\circ 3$	$\circ 2$	$\circ 1$	$\circ 4$	$\circ 3$	$\circ 2$	$\circ 4$	$\circ 3$	$\circ 1$	$\circ 2$	$\circ 4$
$\bar{2}$	$\bar{1}$	2	3	4	1	$\bar{2}$	$\bar{2}$	1	3	4	2	$\bar{1}$	$\bar{2}$	1	4	3	2	$\bar{1}$	$\bar{1}$	2	4	3	1

Table 4: Representing a coloring of 8-cycle prisms Θ_i ($i = 1, 2, 3, 4$).

On the other hand, Table 4 uses the notation of Table 1 in representing a coloring of the union U of almost four (namely $3\frac{3}{4}$) contiguous 8-cycle prisms Θ_i ($i = 1, 2, 3, 4$) and the resulting forced colors for the departing edges away from U . In Table 4, the middle row sequence, call it Υ (obtained by disregarding the symbols “ \square ”, or replacing them by commas) represents the subsequences of colors of the edges $\{(0, u), (1, u)\}$ in the prisms Θ_i namely the subsequences $\Upsilon_1 = (1, 2, 3, 4)^2$ $\Upsilon_2 = (3, 4, 2, 1)^2$ $\Upsilon_3 = (2, 1, 4, 3)^2$ and $\Upsilon_4 = (4, 3, 1, 2)^2$. Here, the last two terms of each Υ_i coincide (i.e. are shared) with the first two terms of its subsequent Υ_{i+1} where the last 6-term subsequence is completed to Υ_4 by adding the first two terms of Υ_1 so Υ_1 may be considered as the next Υ_i after the last Υ_4 (and explaining the fraction $3\frac{3}{4}$ mentioned above). This suggest that Υ can be concatenated with itself a number ℓ of times to close a $(24 \times \ell)$ -cycle of colors for the edges $(\{0, u), (1, u)\}$ of a Hamilton-cycle (of Γ') prism H which may be completed to an egc graph Γ by means of the following considerations. (An adequately colored graph Γ' is obtained from Fig. 8(d) by adding a suitable colored outer cycle, missing in the figure).

On the top and bottom rows of Table 4, the colors 1, 2, 3 and 4 with a bar on top are those of the “long” edges in the four prisms Θ_i that close the two 8-cycles in each Θ_i . The remaining (non-barred) colors suggest that the corresponding edges form external 4-cycles that may be joined with H to form a Γ as desired. The “even longer” edges of these external

4-cycles must be set to form (with two edges of the form $\{(0, u), (1, u)\}$) new 4-cycles and can be selected to form the desired Γ by taking the number of concatenated copies of U to be $\ell = 4$ so that $|V(\Gamma)| = 192$. The two columns in Table 4 whose transpose rows are “ $4 \circ 3 \circ 2$ ” and “ $4 \circ 1 \circ 2$ ”, namely the third leftmost and seventh rightmost \square -free columns, integrate one such 4-cycle. The leftmost third, fourth, fifth and sixth columns are paired this way with the rightmost seventh, eighth, ninth and tenth columns, but the last three pairs must be paired with similar columns in the second, third and fourth version of Table 4 (for indices $k \in \{2, 3, 4 = \ell\}$ of copies U_k of U if we agree that the leftmost third and rightmost seventh columns above are both for $k = 1$ and $U = U_k = U_1$). The same treatment can be set from the leftmost ninth, tenth, eleventh and twelfth respectively to the rightmost first, second, third and fourth columns, which also correspond in pairs that form again “long” 4-cycles.

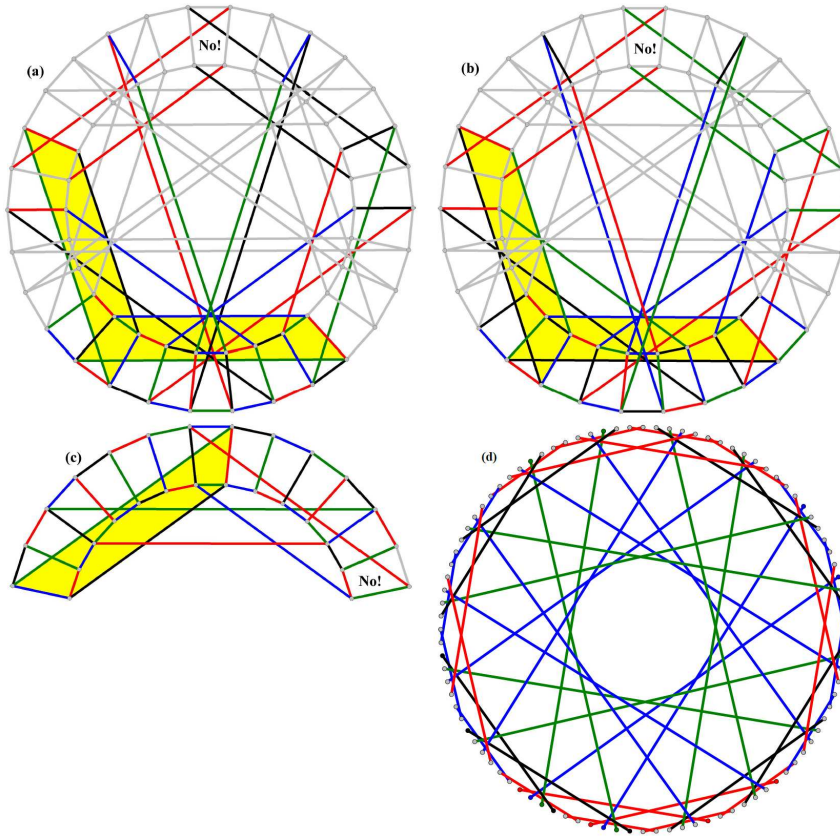


Figure 8: Tutte 8-cage 31^3 -graph prism in (a), (b) and (c), and 96-vertex cubic Γ' in (d), where (a), (b) and (c) show why the 31^3 -graph prism of the Tutte 8-cage is not egc, having five 8-cycle prisms $K_2 \square C_8$ in Γ (presented cyclically mod 5), each of whose vertices should have its four incident edges colored differently. In fact, (a), (b) and (c) present exhaustively without loss of generality partial edge-colorings in Γ with copies of $K_2 \square C_8$ edge-colored accordingly and notification “No!” if an obstruction to edge-coloring continuation appears.

Theorem 21. *For each $4 \leq k \in \mathbb{Z}$ there is an egc 31^3 -graph Γ with $192 \times k$ edges as a prism of a hamiltonian cubic graph Γ' on $96 \times k$ vertices based on g contiguous copies of the*

edge-colored subgraph in Table 4. However, the Tutte 8-cage is a non-egc 31^3 -graph.

Proof. The argument above the statement can be completed for the case $k = 1$. By concatenating the graph from Table 4 any multiple of g times, one extends the construction. \square

Remark 22. The cubic vertex-transitive graphs on less than one hundred vertices with girth 10 and that have egc prisms are in the notation of [21]:

CubicVT[80,30], CubicVT[96,34], CubicVT[96,49], CubicVT[96,50] and CubicVT[96,62].

5 EgC 1111-graphs

A construction [31] of 1^4 -graphs, also called *girth-tight* [23], proceeds as follows. Let Γ be 4-regular and let \mathcal{C} be a partition of $E(\Gamma)$ into cycles. The pair (Γ, \mathcal{C}) is a *cycle decomposition* of Γ . Two edges of Γ are *opposite* at vertex v if both are incident to v and belong to the same element of \mathcal{C} . The *partial line graph* $\mathbb{P}(\Gamma, \mathcal{C})$ of (Γ, \mathcal{C}) is the graph with the edges of Γ as vertices, and any two such vertices adjacent if they share, as edges, a vertex of Γ and are not opposite at that vertex. A cycle C in Γ is \mathcal{C} -*alternating* if no two consecutive edges of C belong to the same element of \mathcal{C} . Lemma 4.10 [23] says that $\mathbb{P}(\Gamma, \mathcal{C})$ is girth-tight if and only if (Γ, \mathcal{C}) contains neither \mathcal{C} -alternating cycles nor triangles, except those contained in \mathcal{C} .

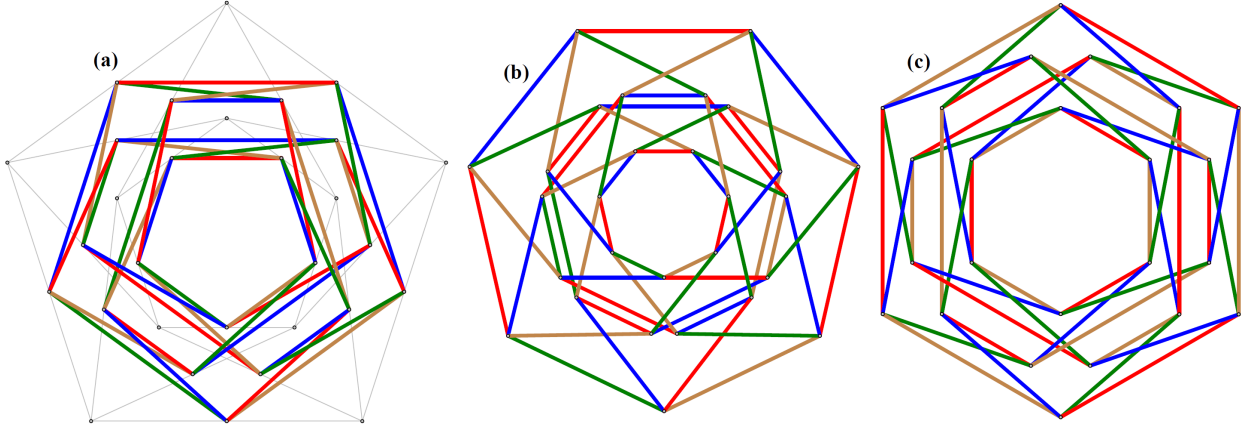


Figure 9: Tight factorizations of $\mathbb{P}(W(5, 2))$, $\mathbb{P}(W(7, 2))$ and $\mathbb{P}(W(6, 2))$.

Example 23. As initial example of a partial line graph, consider the wreath graph $W(n, 2) = C_n[\overline{K_2}]$ ($n > 4$), where C_n is a cycle $(v_0, v_1, \dots, v_{n-1})$. Consider the partition \mathcal{C} of $W(n, 2)$ into the 4-cycles $((v_i, 0), (v_{i+1}, 0), (v_i, 1), (v_{i+1}, 1))$ ($i \in \mathbb{Z}_n$). These form a decomposition $(W(n, 2), \mathcal{C})$ which yields the partial line graph $\mathbb{P}(W(n, 2), \mathcal{C})$. We prove now that for all values of n $\mathbb{P}(W(n, 2), \mathcal{C})$ is egc, as in Fig. 9(a–c), where $\mathbb{P}(W(5, 2), \mathcal{C})$, $\mathbb{P}(W(7, 2), \mathcal{C})$ and $\mathbb{P}(W(6, 2), \mathcal{C})$ are represented, showing tight factorizations via edge colors 1, 2, 3, 4.

Theorem 24. Let $4 < n \in \mathbb{Z}$. Then, $\mathbb{P}(W(n, 2), \mathcal{C})$ is egc.

Proof. Each vertex $((v_i, j)(v_{i\pm 1}, j'))$ of $\mathbb{P}(W(n, 2), \mathcal{C})$ representing the edge between the vertices (v_i, j) and $(v_{i\pm 1}, j')$ of $W(n, 2)$ where $i \in \mathbb{Z}_n$ and $j, j' \in \{0, 1\}$ will be denoted $(i_j(i\pm 1)_{j'})$.

We use modifications of Lemma 9 separately for the cases of odd and even n . If $n = 2k + 1$ is odd, then we have a 2-factorization of $\mathbb{P}(W(n, 2), \mathcal{C})$ one of whose two 2-factors is composed by three disjoint even-length cycles not sharing more than two edges with any 4-cycle, namely one of length 8 and two of length $4k + 2$ specifically:

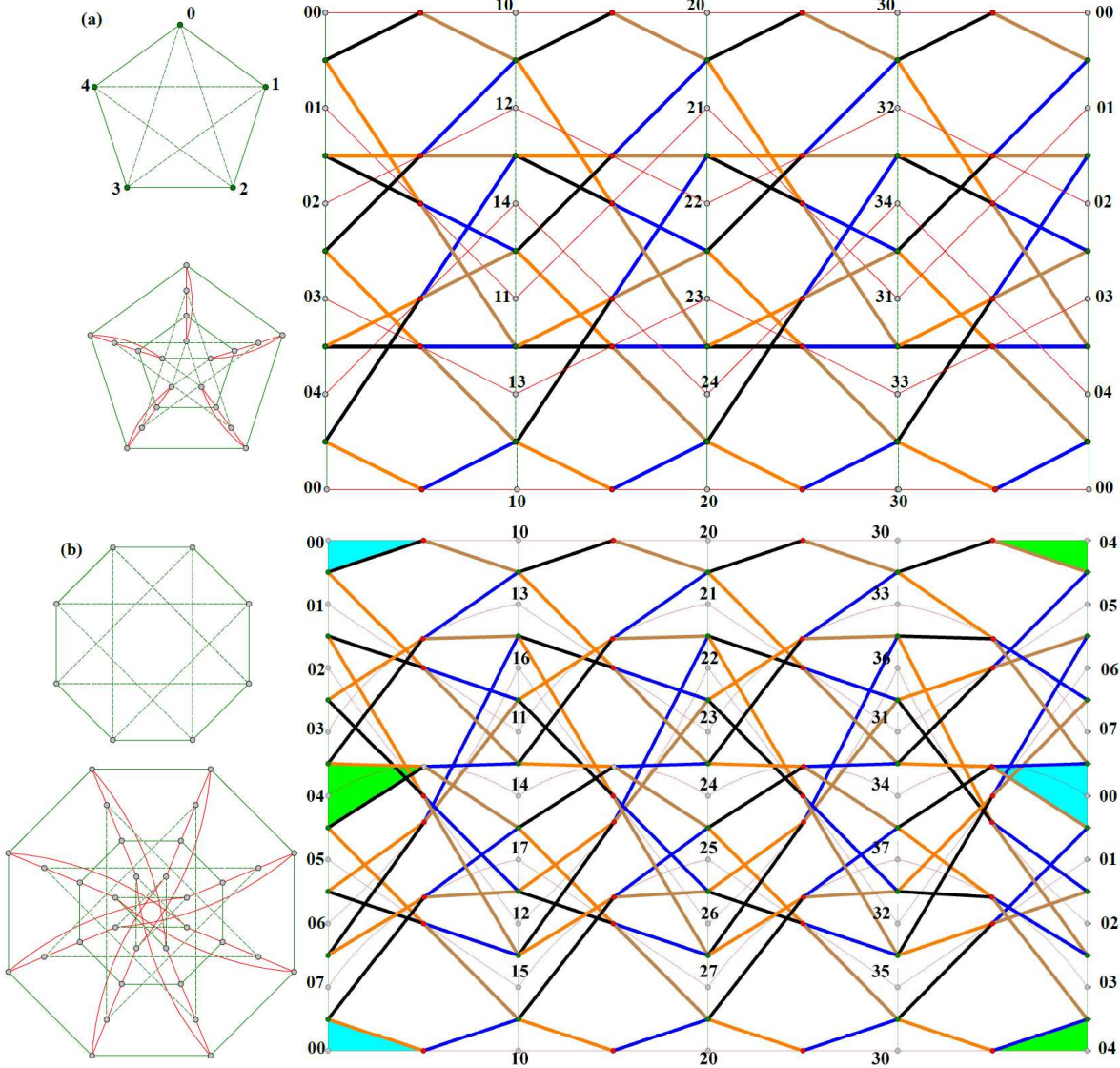


Figure 10: Tight factorizations of (a) $\mathbb{P}(\text{Br}(4, 5; 2))$ and (b) $\mathbb{P}(\text{MBr}(4, 8; 3))$.

$$\begin{aligned}
 &((-k_0 k_0)(-k_0(1-k)_1)(-k_0 k_1)((k-1)_0 k_1)(-k_1 k_1)(-k_1(1-k)_0)(-k_1 k_0)((k-1)_1 k_0)); \\
 &((-k_0(1-k)_0) \cdots (-1_0 0_0)(0_0 1_0) \cdots ((k-1)_0 k_0)(k_0(k-1)_1) \cdots (1_1 0_1)(0_1 - 1_1) \cdots (k_1 - k_0)); \\
 &((-k_1(1-k)_1) \cdots (-1_1 0_1)(0_1 1_1) \cdots ((k-1)_1 k_1)(k_1(k-1)_0) \cdots (1_0 0_0)(0_0 - 1_0) \cdots (k_0 - k_1)),
 \end{aligned}$$

which for $k = 2$ and $k = 3$ can be visualized respectively in Fig. 9(a) and Fig. 9(b) as three alternate-red-blue cycles, one of length 8 and two of length $4k + 2$. The other 2-factor

also is formed by even cycles not sharing more than two edges with any 4-cycle, viewable as alternate-green-hazel cycles for $k = 2$ in Fig. 9(a) and for $k = 3$ in Fig. 9(b). This 2-factor has reflective \mathbb{Z}_2 symmetry on a vertical axis. As for the mentioned modifications of Lemma 9, note that the two cycles of length $4k + 2$ differ, either for k odd or for k even differ: If k is odd, the two cycles of length $2k + 2$ contain opposite edges in the 4-cycles, while if k is even, the two cycles of length $2k + 2$ share just one edge with each 4-cycle. Both cases refine into corresponding tight 1-factorizations. In particular, if $n = 2k$ is even, then a 2-factorization of $\mathbb{P}(W(n, 2), \mathcal{C})$ is formed by k cycles of length 8 forming a class of cycles (mod k) namely

$$((i_0(i+1)_0)((i+1)_0(i+2)_0)((i+2)_0(i+1)_1)((i+1)_1i_0)((i+1)_1i_1)((i+1)_1(i+2)_1)((i+2)_1(i+1)_0)((i+1_0)i_1)),$$

where i is odd, $0 < i < n$. The other 2-factor also is formed by 8-cycles, see Fig. 9(c). \square

In order to obtain additional girth-tight graphs with tight factorizations, we recur to a particular case of a cycle decomposition known as *linking-ring structure* [31], that works for two colors, say red and green. This structure applies in the following paragraphs only for n even; (if n is odd, then more than two colors would be needed in order to distinguish adjacent cycles of the decomposition $(W(n, 2), \mathcal{C})$). A *linking-ring structure* is defined in items (i)–(iii) below, as follows. An *isomorphism between two cycle decompositions* $(\Gamma_1, \mathcal{C}_1)$ and $(\Gamma_2, \mathcal{C}_2)$ is an isomorphism $\xi : \Gamma_1 \rightarrow \Gamma_2$ such that $\xi(\mathcal{C}_1) = \mathcal{C}_2$. An isomorphism ξ from a cycle decomposition to itself is an *automorphism*, written $\xi \in \text{Aut}(\Gamma, \mathcal{C})$. A cycle decomposition (Γ, \mathcal{C}) is *flexible* if for every vertex v and each edge e incident to v there is $\xi \in \text{Aut}(\Gamma, \mathcal{C})$ such that:

- (I) ξ fixes each vertex of the cycle in \mathcal{C} containing e and
- (II) ξ interchanges the two other neighbors of v ; the edges joining v to those neighbors are in some other cycle of \mathcal{C} .

A cycle decomposition (Γ, \mathcal{C}) is *bipartite* if \mathcal{C} can be partitioned into two subsets \mathcal{G} (green) and \mathcal{R} (red) so that each vertex of Γ is in one cycle of \mathcal{G} and one cycle of \mathcal{R} .

The largest subgroup of $\text{Aut}(\Gamma, \mathcal{C})$ preserving each of the sets $\mathcal{C}_1 = \mathcal{G}$ (\mathcal{G} for “green”), and $\mathcal{C}_2 = \mathcal{R}$ (\mathcal{R} for “red”), is denoted $\text{Aut}^+(\Gamma, \mathcal{C})$. In a bipartite cycle decomposition, an element of $\text{Aut}(\Gamma, \mathcal{C})$ either interchanges \mathcal{G} and \mathcal{R} or preserves each of \mathcal{G} and \mathcal{R} set-wise, so it is contained in $\text{Aut}^+(\Gamma, \mathcal{C})$. This shows that the index of $\text{Aut}^+(\Gamma, \mathcal{C})$ in $\text{Aut}(\Gamma, \mathcal{C})$ is at most 2. If this index is 2, then we say that (Γ, \mathcal{C}) is *self-dual*; this happens if and only if there is $\sigma \in \text{Aut}(\Gamma, \mathcal{C})$ such that $\mathcal{G}\sigma = \mathcal{R}$ and $\mathcal{R}\sigma = \mathcal{G}$. In [23], a cycle decomposition (Γ, \mathcal{C}) is said to be a *linking-ring (LR) structure* if it is

- (i) bipartite,
- (ii) flexible and
- (iii) $\text{Aut}^+(\Gamma, \mathcal{C})$ acts transitively on $V(\Gamma)$.

However, there are tight factorizations of girth-tight graphs $\mathbb{P}(\Gamma, \mathcal{P})$ obtained by relaxing condition (iii) in that definition. So we will say that a cycle decomposition (Γ, \mathcal{P}) is a *relaxed LR structure* if it satisfies just conditions (i) and (ii).

$(0_1^0[a]_1^0 1[b] 0_2^1[c]_0^3 1[d])$	$(1_2^0[a]_2^1 2[b] 1_4^2[c]_1^0 2[d])$	$(2_1^0[a]_3^2 1[b] 2_2^1[c]_2^1 1[d])$	$(3_2^0[a]_0^3 2[b] 3_4^2[c]_3^2 2[d])$
$(0_2^1[a]_1^0 2[b] 0_3^2[c]_0^3 2[d])$	$(1_3^1[a]_2^1 3[b] 1_0^3[c]_0^0 3[d])$	$(2_2^1[a]_3^2 2[b] 2_3^2[c]_2^1 2[d])$	$(3_3^1[a]_0^3 3[b] 3_0^3[c]_3^3 3[d])$
$(0_3^2[a]_1^0 3[b] 0_4^3[c]_0^3 3[d])$	$(1_4^2[a]_2^1 4[b] 1_1^4[c]_1^0 4[d])$	$(2_3^2[a]_3^3 3[b] 2_4^3[c]_2^1 3[d])$	$(3_4^2[a]_0^4 4[b] 3_1^4[c]_3^2 4[d])$
$(0_4^3[a]_1^0 4[b] 0_0^4[c]_0^3 4[d])$	$(1_0^3[a]_2^1 0[b] 1_2^0[c]_1^0 0[d])$	$(2_4^3[a]_3^4 4[b] 2_0^4[c]_2^1 4[d])$	$(3_0^3[a]_0^0 0[b] 3_2^0[c]_3^2 0[d])$
$(0_0^4[a]_1^0 0[b] 0_1^0[c]_0^3 0[d])$	$(1_1^4[a]_2^1 1[b] 1_3^1[c]_1^0 1[d])$	$(2_0^4[a]_3^0 0[b] 2_1^0[c]_2^1 0[d])$	$(3_1^0[a]_0^1 1[b] 3_3^1[c]_3^2 1[d])$

Table 5: A code representation of the tight factorization in Fig. 10(a).

Remark 25. With the aim of yielding semisymmetric graphs from LR structures, [31] defines:

- (a) the *barrel* $\text{Br}(k, n; r)$ where $4 \leq k \equiv 0 \pmod{2}$ $n \geq 5$ $r^2 \equiv \pm 1 \pmod{n}$ $r \not\equiv \pm 1 \pmod{n}$ and $0 \leq r < \frac{n}{2}$ as the graph with vertex set $\mathbb{Z}_k \times \mathbb{Z}_n$ and (i, j) red-adjacent to $(i \pm 1, j)$ and green-adjacent to $(i, j \pm r^i)$;
- (b) the *mutant barrel* $\text{MBr}(k, n; r)$ where $2 \leq k \equiv n \equiv 0 \pmod{2}$ $n \geq 6$ $r^2 \equiv \pm 1 \pmod{n}$ and $r \not\equiv \pm 1 \pmod{n}$ as the graph with vertex set $\mathbb{Z}_k \times \mathbb{Z}_n$ and (i, j) red-adjacent to $(i + 1, j)$ for $0 \leq i < k - 1$ $(k - 1, j)$ red-adjacent to $(0, j + \frac{n}{2})$ and (i, j) green-adjacent to $(i, j \pm r^i)$.

The right side of Fig. 10(a) (resp. 10(b)) represents $\mathbb{P}(\text{Br}(4, 5; 2))$ (resp. $\mathbb{P}(\text{MBr}(4, 8; 3))$), where:

- (i) each vertex (i, j) is denoted ij ,
- (ii) vertices $i0$ appear twice (on top and bottom, to be identified for each i),
- (iii) red edges are shown in thin trace,
- (iv) green edges arising from the cycles $F_1^5 = (0, 1, 2, 3, 4)$ and $F_2^5 = (0, 2, 4, 1, 3)$ of K_5 (resp. $F_1^8 = (0, 1, 2, 3, 4, 5, 6, 7)$ and $F_3^8 = (0, 3, 6, 1, 4, 7, 2, 5)$ of K_8) are shown in thin and dashed trace, respectively, and
- (v) the edges of the corresponding partial line graphs are shown in thick trace on the colors orange = a , black = b , hazel = c and blue = d , setting a tight factorization.

Vertices of green and red cycles are said to be *green* and *red*, respectively. To the left of these two graphs in Fig. 10, the corresponding green and red-green subgraphs are shown.

Note that thick edges of colors orange and black form cycles zigzagging between:

- (A) the vertices of each vertical green cycle (excluding the rightmost green cycle) and
- (B) their adjacent red vertices to their immediate right.

Also, note that thick blue and hazel edges form cycles zigzagging between:

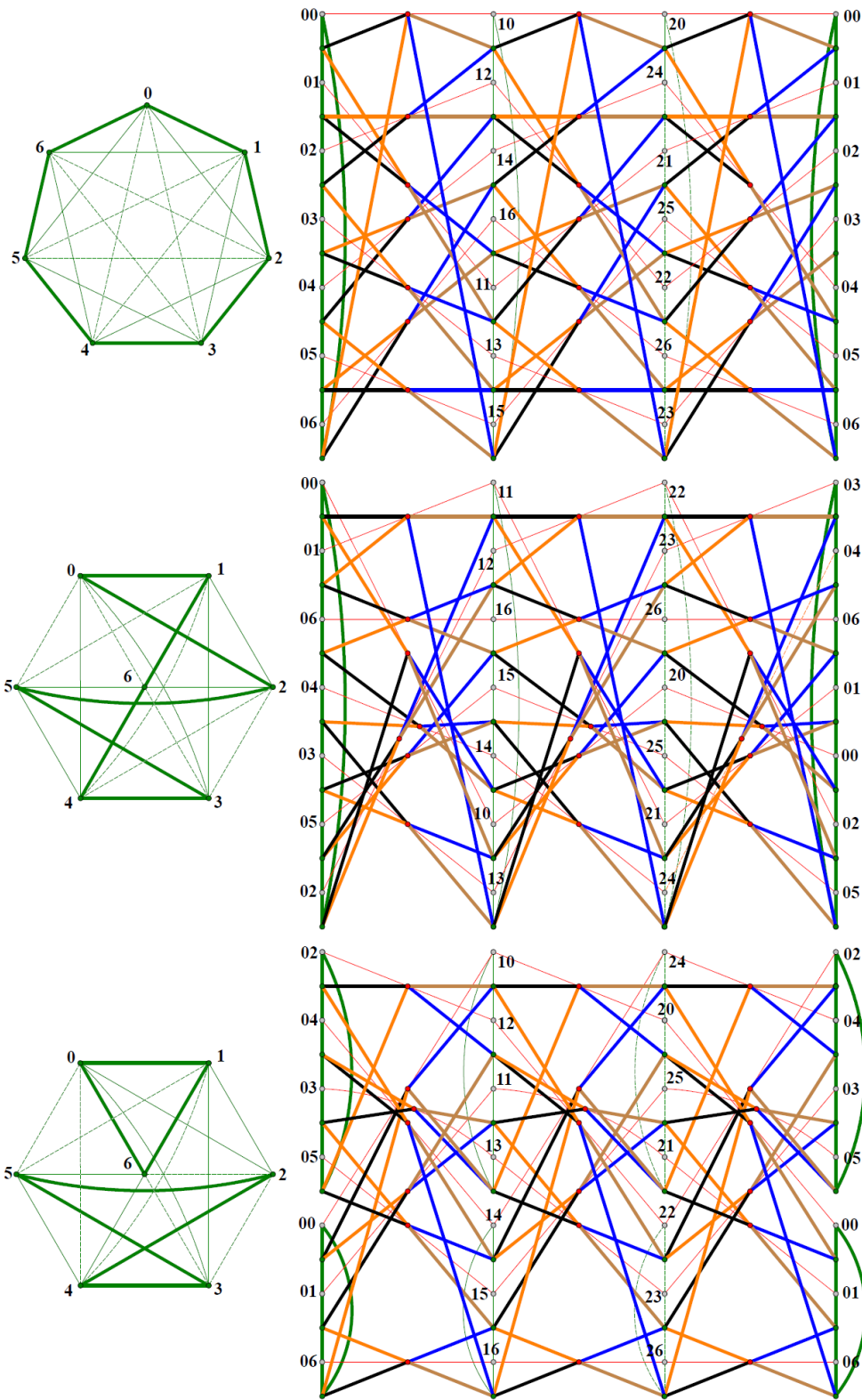


Figure 11: Egc $\mathbb{P}(\text{Br}(3, F))$ for the three 2-factorizations F of K_7 .

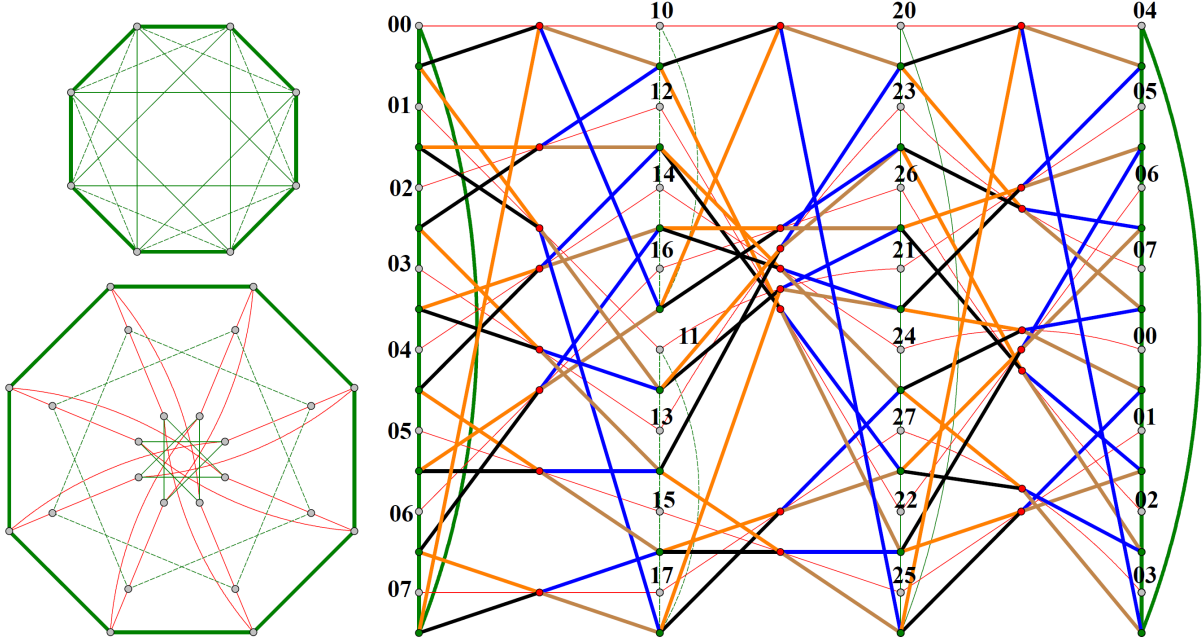


Figure 12: Tight factorization of $\mathbb{P}(\text{MBr}(3, \{F_1^8, F_2^8, F_3^8\}))$ based on 2-factors of K_8 .

$(0_1^0[a]_1^0 1[b]_0 0_2^1[c]_0^2 1[d])$	$(1_2^0[c]_1^0 2[d] 1_4^2[a]_2 2[b])$	$(2_3^0[a]_0^2 3[b] 2_6^3[c]_2 3[d])$
$(0_2^1[a]_1^0 2[b] 0_3^2[c]_0^2 2[d])$	$(1_3^1[c]_1^0 3[d] 1_5^3[a]_2 3[b])$	$(2_4^1[a]_0^2 4[b] 2_0^4[c]_2 4[d])$
$(0_3^2[a]_1^0 3[b] 0_4^3[c]_0^2 3[d])$	$(1_4^2[c]_1^0 4[d] 1_6^4[a]_2 4[b])$	$(2_5^2[a]_0^2 5[b] 2_1^5[c]_2 5[d])$
$(0_4^3[a]_1^0 4[b] 0_5^4[c]_0^2 4[d])$	$(1_5^3[c]_1^0 5[d] 1_0^5[a]_2 5[b])$	$(2_6^3[a]_0^2 6[b] 2_2^6[c]_2 6[d])$
$(0_5^4[a]_1^0 5[b] 0_6^5[c]_0^2 5[d])$	$(1_6^4[c]_1^0 6[d] 1_1^6[a]_2 6[b])$	$(2_0^4[a]_0^2 0[b] 2_3^4[c]_2 0[d])$
$(0_6^5[a]_1^0 6[b] 0_0^6[c]_0^2 6[d])$	$(1_0^5[c]_1^0 0[d] 1_2^0[a]_2 0[b])$	$(2_1^5[a]_0^2 1[b] 2_4^1[c]_2 1[d])$
$(0_0^6[a]_1^0 0[b] 0_1^0[c]_0^2 0[d])$	$(1_1^6[c]_1^0 1[d] 1_3^1[a]_2 1[b])$	$(2_2^6[a]_0^2 2[b] 2_5^2[c]_2 2[d])$
$(0_1^0[a]_1^0 1[b] 0_5^1[c]_0^2 5[d])$	$(1_2^1[c]_1^0 2[d] 1_0^2[a]_2 0[b])$	$(2_3^2[a]_0^2 3[b] 2_1^3[c]_2 1[d])$
$(0_5^1[a]_1^0 5[b] 0_2^2[c]_0^2 2[d])$	$(1_0^2[c]_1^0 0[d] 1_3^0[a]_2 3[b])$	$(2_1^3[a]_0^2 1[b] 2_4^1[c]_2 4[d])$
$(0_2^2[a]_1^0 2[b] 0_4^2[c]_0^2 4[d])$	$(1_3^0[c]_1^0 3[d] 1_5^3[a]_2 5[b])$	$(2_4^1[a]_0^2 4[b] 2_0^4[c]_2 0[d])$
$(0_4^2[a]_1^0 4[b] 0_3^3[c]_0^2 3[d])$	$(1_5^3[c]_1^0 5[d] 1_4^5[a]_2 4[b])$	$(2_0^4[a]_0^2 0[b] 2_5^4[c]_2 5[d])$
$(0_3^3[a]_1^0 3[b] 0_6^3[c]_0^2 6[d])$	$(1_4^5[c]_1^0 4[d] 1_6^4[a]_2 6[b])$	$(2_5^4[a]_0^2 5[b] 2_6^5[c]_2 6[d])$
$(0_6^3[a]_1^0 6[b] 0_0^6[c]_0^2 0[d])$	$(1_6^4[c]_1^0 6[d] 1_1^6[a]_2 1[b])$	$(2_6^5[a]_0^2 6[b] 2_2^6[c]_2 2[d])$
$(0_0^6[a]_1^0 0[b] 0_1^0[c]_0^2 1[d])$	$(1_1^6[c]_1^0 1[d] 1_2^1[a]_2 2[b])$	$(2_2^6[a]_0^2 2[b] 2_3^2[c]_2 3[d])$
$(0_1^0[a]_1^0 1[b] 0_6^1[c]_0^2 6[d])$	$(1_3^1[c]_1^0 3[d] 1_1^3[a]_2 1[b])$	$(2_0^2[a]_0^2 2[b] 2_1^2[c]_2 1[d])$
$(0_6^1[a]_1^0 6[b] 0_0^6[c]_0^2 6[d])$	$(1_1^3[c]_1^0 1[d] 1_5^1[a]_2 5[b])$	$(2_1^2[a]_0^2 1[b] 2_4^1[c]_2 4[d])$
$(0_0^6[a]_1^0 0[b] 0_1^0[c]_0^2 0[d])$	$(1_5^1[c]_1^0 5[d] 1_0^5[a]_2 0[b])$	$(2_4^1[a]_0^2 4[b] 2_0^4[c]_2 0[d])$
$(0_3^0[a]_1^0 3[b] 0_4^3[c]_0^2 3[d])$	$(1_0^5[c]_1^0 0[d] 1_3^0[a]_2 3[b])$	$(2_0^4[a]_0^2 0[b] 2_0^4[c]_2 2[d])$
$(0_4^3[a]_1^0 4[b] 0_5^4[c]_0^2 4[d])$	$(1_2^4[c]_1^0 4[d] 1_6^4[a]_2 6[b])$	$(2_5^4[a]_0^2 5[b] 2_6^5[c]_2 6[d])$
$(0_5^4[a]_1^0 5[b] 0_2^5[c]_0^2 5[d])$	$(1_6^4[c]_1^0 6[d] 1_2^6[a]_2 2[b])$	$(2_6^5[a]_0^2 6[b] 2_3^6[c]_2 3[d])$
$(0_2^5[a]_1^0 2[b] 0_3^2[c]_0^2 2[d])$	$(1_2^6[c]_1^0 2[d] 1_4^2[a]_2 4[b])$	$(2_3^6[a]_0^2 2[b] 2_5^3[c]_2 5[d])$

Table 6: Code representations of F_1^7 , F_2^7 and F_3^7 .

(C) the red vertices and

(D) the vertices of the next vertical green cycle to their right.

The girth is realized by 4-cycles with the four colors, with a pair of edges (blue and hazel) to the left of each vertical green cycle and another pair of edges (black and orange) to the corresponding right. This is always attainable, because similar bicolored cycles can always be obtained, generating the desired tight factorizations. For instance, assigning colors a, b, c, d to the edges $(i_j^{j+r^i}, i^{i+1}j)$ $(i_j^{j+r^i}, i^{i+1}(j+r^i))$ $((i+1)_j^{j+r^i}, i^{i+1}(j+r^i))$ and $((i+1)_j^{j+r^i}, i^{i+1}j)$ respectively, yields a tight factorization of $\mathbb{P}(\text{Br}(k, n; r))$.

$(0_1^0[a]_1^01[b]0_2^1[c]_0^31[d])$	$(1_2^0[a]_2^12[b]1_4^2[c]_1^02[d])$	$(2_3^0[a]_3^23[b]2_6^3[c]_2^13[d])$	$(3_4^0[a]_4^34[b]3_8^4[c]_3^24[d])$
$(0_2^1[a]_1^02[b]0_3^2[c]_0^32[d])$	$(1_3^1[a]_2^13[b]1_5^3[c]_1^03[d])$	$(2_4^1[a]_3^24[b]2_7^4[c]_2^14[d])$	$(3_5^1[a]_0^35[b]3_0^5[c]_3^25[d])$
$(0_3^2[a]_0^13[b]0_4^3[c]_0^33[d])$	$(1_4^2[a]_2^14[b]1_6^4[c]_0^14[d])$	$(2_5^2[a]_3^25[b]2_8^5[c]_2^15[d])$	$(3_6^2[a]_0^36[b]3_1^6[c]_3^26[d])$
$(0_4^3[a]_1^04[b]0_5^4[c]_0^34[d])$	$(1_5^3[a]_2^15[b]1_7^5[c]_0^15[d])$	$(2_6^3[a]_3^26[b]2_0^6[c]_2^16[d])$	$(3_7^3[a]_0^37[b]3_2^7[c]_3^27[d])$
$(0_5^4[a]_1^05[b]0_6^5[c]_0^35[d])$	$(1_6^4[a]_2^16[b]1_8^6[c]_0^16[d])$	$(2_7^4[a]_3^27[b]2_1^7[c]_2^17[d])$	$(3_8^4[a]_0^38[b]3_3^8[c]_3^28[d])$
$(0_6^5[a]_0^16[b]0_7^6[c]_0^36[d])$	$(1_8^5[a]_2^17[b]1_0^8[c]_0^17[d])$	$(2_8^5[a]_3^28[b]2_2^8[c]_2^18[d])$	$(3_0^5[a]_0^30[b]3_4^9[c]_3^20[d])$
$(0_7^6[a]_0^17[b]0_8^7[c]_0^37[d])$	$(1_0^6[a]_2^18[b]1_1^8[c]_0^18[d])$	$(2_0^6[a]_3^20[b]2_3^0[c]_2^10[d])$	$(3_1^6[a]_0^31[b]3_5^9[c]_3^21[d])$
$(0_8^7[a]_0^18[b]0_0^8[c]_0^38[d])$	$(1_1^7[a]_2^10[b]1_2^0[c]_0^10[d])$	$(2_1^7[a]_3^21[b]2_4^1[c]_2^11[d])$	$(3_2^7[a]_0^32[b]3_6^9[c]_3^22[d])$
$(0_0^8[a]_0^10[b]0_0^9[c]_0^30[d])$	$(1_2^8[a]_2^11[b]1_3^1[c]_0^11[d])$	$(2_2^8[a]_3^22[b]2_5^2[c]_2^12[d])$	$(3_3^8[a]_0^33[b]3_7^9[c]_3^23[d])$

Table 7: Tight factorization of $\mathbb{P}(4, F^9)$.

A code representation of the tight factorization in Fig. 10(a) is given in Table 5, where each green edge $\{ij, i(j+r^i)\}$ in $\text{Br}(k, n; r)$ yields a green vertex $i_j^{j+r^i}$ in $\mathbb{P}(\text{Br}(k, n; r))$ each red edge $\{ij, (i+1)j\}$ in $\text{Br}(k, n; r)$ yields a red vertex $i^{i+1}j$ in $\mathbb{P}(\text{Br}(k, n; r))$ and the color of an edge between a green vertex and a red vertex is indicated between brackets: $[a]$ for orange, $[b]$ for black, $[c]$ for hazel and $[d]$ for blue.

Remark 26. Generalizing Remark 25 to get other egc girth-tight graphs, we consider a 2-factorization $F^n = \{F_1^n, F_2^n, \dots, F_{k-1}^n\}$ of the complete graph K_n for odd $n = 2k + 1 > 6$ and use it to define the *barrel* $\text{Br}(k, F^n)$ with

(i) $\mathbb{Z}_k \times \mathbb{Z}_n$ as vertex set and

(ii) edges forming precisely red cycles $((0, i), (1, i), \dots, (k-1, i))$ where $i \in \mathbb{Z}_n$ and green subgraphs $\{j\} \times F_j^n$ where $j \in \mathbb{Z}_k$.

Fig. 11 contains representations of $\mathbb{P}(\text{Br}(3, F^7))$ for three distinct 2-factorizations F^7 of K_7 with tight factorizations represented as in Fig. 10, with green cycles so that each vertex $(i, 0) = i0$ appears just once (not twice, as in Fig. 10(a–b)). In the three cases, F_1^7 , F_2^7 and F_3^7 green edges are traced thick, thin and dashed, respectively. To the left of these representations, the corresponding green subgraphs are shown. Code representations of these three tight factorizations can be found in Table 6, following the conventions of Table 5.

(A different 1-factorization of K_7 that may be used with the same purpose is for example $\{(0, 1, 2, 3, 4, 5, 6), (0, 3, 5, 1, 6, 2, 4), (0, 2, 5)(1, 3, 6, 4)\}$).

In the same way, by considering the 2-factorization given in K_9 seen as the Cayley graph $C_9(1, 2, 3, 4)$ with F^9 formed by the 2-factors $F_1^9, F_2^9, F_3^9, F_4^9$ generated by the respective colors 1, 2, 3, 4, namely Hamilton cycles F_1^9, F_2^9, F_4^9 but $F_3^9 = 3K_3$ we get a tight factorization of $\mathbb{P}(4, F^9)$. This is encoded in Table 7 in a similar fashion to that of Tables 4–5.

If $n = 2k$ is even, a similar generalization takes a 2-factorization $F^n = \{F_1^n, F_2^n, \dots, F_{k-2}^n\}$ of $K_n - \{i(i+k); i = 0, \dots, k-1\}$ and uses the 1-factor $\{i(i+k); i = 0, \dots, k-1\}$ to get a generalized *mutant barrel* $\text{MBr}(k-1, F^n)$ in a likewise fashion to that of item (b) in Remark 25 but modified now via F^n namely with

(i') $\mathbb{Z}_{k-1} \times \mathbb{Z}_n$ as vertex set and

(ii') edges forming precisely red cycles $((0, i), (1, i), \dots, (k-1, i), (0, i + \frac{n}{2}), (1, i + \frac{n}{2}), \dots, (k-1, i + \frac{n}{2}))$ where $i \in \mathbb{Z}_n$ and green subgraphs $\{j\} \times F_j^n$ where $j \in \mathbb{Z}_k$.

Fig. 12 represents a tight factorization of $\mathbb{P}(\text{MBr}(3, F^8))$ where $F^8 = \{F_1^8, F_2^8, F_3^8\}$ represented on the upper left of the figure, is such a 2-factorization, with F_1^8 and F_3^8 as in Fig. 10, and $F_2^8 = (0, 2, 4, 6)(1, 3, 5, 7)$ via corresponding thick, thin and dashed, green edge tracing. On the lower left, a representation of the red-green graph $\text{MBr}(3, F^8)$ is found.

We can further extend these notions of barrel and mutant barrel by taking a cycle $G^n = (G_1^n, G_2^n, \dots, G_\ell^n)$ of copies of the 2-factors of F^n where $G_i^n \in F^n$ but with no two contiguous G_i^n and $G_{i+1}^n \pmod n$ being the same element of F^n . Here, $\ell \geq 3$. This defines a barrel $\text{Br}(\ell, G^n)$ or mutant barrel $\text{MBr}(\ell, G^n)$ (n even in this case) and establishes the following.

Theorem 27. *The barrels and mutant barrels obtained in Remark 26 produce corresponding egc graphs $\mathbb{P}(\text{Br}(\ell, G^n))$ and $\mathbb{P}(\text{MBr}(\ell, G^n))$.*

Proof. The zigzagging orange-black and hazel-blue cycles between each pair of contiguous green-vertex and red-vertex columns in the graphs of Fig. 10–12 are as in Lemma 9. \square

6 Egc girth-g-regular graphs, g larger than 4

Theorem 28. *We have the following:*

- (a) *the 32-vertex Armanios-Wells graph AW [3] [4, p. 266] is an egc $(12)^5$ -graphs;*
- (b) *the 36-vertex Sylvester graph Syl [4, p. 223] is a 8^5 -graph, but is not egc.*

Proof. (a) The center of Fig. 13 represents AW colored as claimed. The vertices of AW are denoted Xi ($X \in \{A, B, C, D\}; i \in \mathbb{Z}_8$). An edge-color assignment for AW is generated mod 4 or $(\text{mod } \mathbb{Z}_4)$ where $\mathbb{Z}_4 = \{0, 2, 4, 6\} \subset \mathbb{Z}_8$ is a subgroup and an ideal of \mathbb{Z}_8 as follows:

<i>Red</i>	1	(A0, C7)	(A1, C2)	(B0, D1)	(B1, D2)	(6)
<i>Black</i>	2	(A0, C1)	(A1, C0)	(B0, B3)	(D0, D1)	
<i>Blue</i>	3	(A0, D6)	(A1, B4)	(B1, C6)	(C1, D3)	
<i>Hazel</i>	4	(A0, B3)	(A1, D7)	(B0, C5)	(C0, D2)	
<i>Green</i>	5	(A0, C6)	(A1, C7)	(B0, B5)	(D1, D2)	

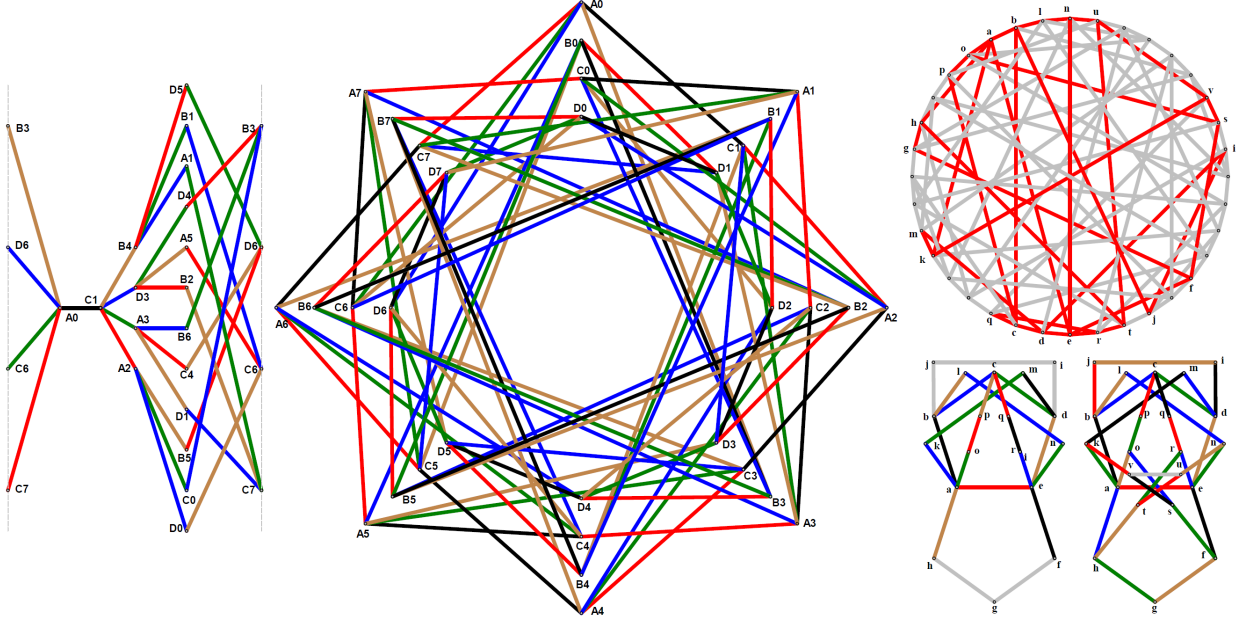


Figure 13: The egc Armanios-Wells $(12)^5$ -graph and the non-egc Sylvester 8^4 -graph.

where indices are taken (mod 8) so colored-edge orbits (mod 4) are either of the form

$$\{(X0, Yi), (X2, Y(i+2)), (X4, Y(i+4)), (X6, Y(i+6))\} \text{ or of the form:} \\ \{(X1, Yj), (X3, Y(j+2)), (X5, Y(j+4)), (X7, Y(j+6))\}$$

with $X, Y \in \{A, B, C, D\}$ $i, j \in \mathbb{Z}_8$ and addition taken (mod 8). The left of Fig. 13 contains the subgraph of AW spanned by the twelve 5-cycles through the black edge $(A0, C1)$ (where the two dashed lines must be identified), showing the disposition of twelve 5-cycles around an edge of AW. Moreover, the four black edges in the second line of (6) represent forty-eight tightly colored 5-cycles, (twelve passing through each black edge, corresponding to the $\frac{5!}{2 \times 5} = 12$ existing color cycles

$$(23451), (23541), (24351), (24531), (25341), (25431), \\ (24513), (25413), (25134), (24135), (23514), (25143))$$

and each such cycle yields an orbit of four such 5-cycles. Since each edge of AW passes through twelve 5-cycles of AW and $|E(AW)| = 80$ we count 80×12 5-cycles in AW with repetitions. Each 5-cycle in this count is repeated five times, so the number of 5-cycles in AW is $(80 \times 12)/5 = 16 \times 12$. Thus, the number of orbits of tightly-colored 5-cycles is 48 and we obtain a tight coloring of AW.

(b) The upper right of Fig. 13 represents Syl with the following 5-cycles:

$$C_0 = (abcde) \quad C_1 = (aefgh) \quad C_2 = (abcmh) \quad C_3 = (cdefg) \quad C_4 = (bcdij) \quad C_5 = (hidea) \\ C_6 = (hijba) \quad C_7 = (cghid) \quad C_8 = (akmde) \quad C_9 = (ablne) \quad C_{10} = (abcpo) \\ C_{11} = (cderq) \quad C_{12} = (aefso) \quad C_{13} = (eahtr) \quad C_{14} = (aksvo) \quad C_{15} = (enutr).$$

The union of C_0, C_1, C_4, C_8, C_9 yields the red subgraph. Coloring tightly C_0, C_8, C_9, C_{10} ,

C_{11} with $\text{color}(ab)=\text{color}(ef)$ and $\text{color}(ah)=\text{color}(de)$ makes impossible continuing coloring tightly C_4 see Syl as shown in the upper right of Fig. 13. Otherwise, in the lower right of Fig. 13 a forced tight coloring of C_0, \dots, C_{12} C_{14} and C_{15} is shown in two representations of the subgraph of Syl induced by these 5-cycles. That leaves C_{13} obstructing a tight-coloring. Thus, Syl is not egc. \square

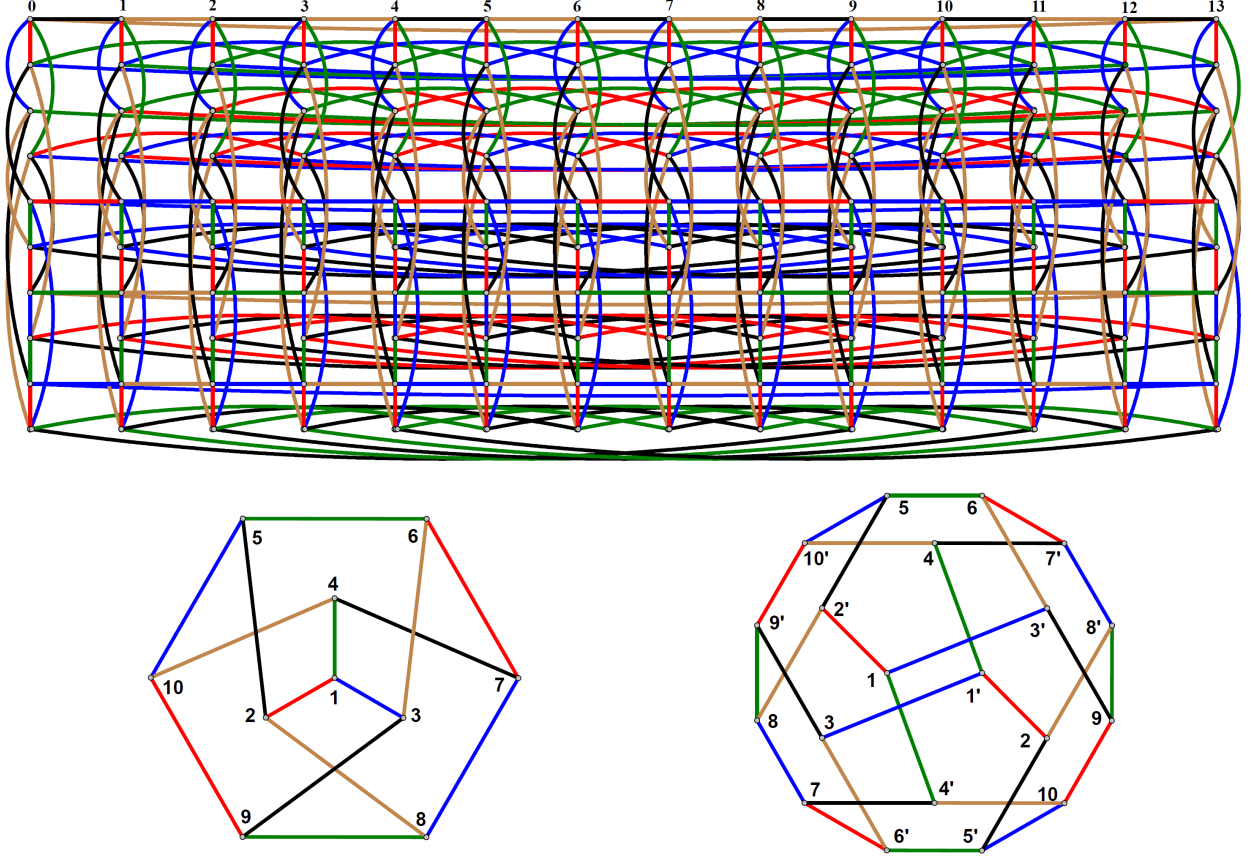


Figure 14: Egc $4^3 0^2$ -graph on 140 vertices; Petersen and dodecahedral graphs.

Subsequently, an egc $4^3 0^2$ -graph Γ is presented by means of a construction that generalizes the barrel constructions used in Section 5, as follows. See the top of Fig. 14, where fourteen vertical copies of the Petersen graph Pet are presented in parallel at equal distances from left to right and numbered from 0 to 13 in \mathbb{Z}_{14} . The vertices of the j -th copy Pet^j of Pet are denoted $v_1^j, v_2^j, \dots, v_{10}^j$ from top to bottom and are joined horizontally by cycles of the Cayley graph of \mathbb{Z}_{14} with generator set $\{1, 3, 5\}$ namely the cycles

$$\begin{aligned}
 & (v_i^0, v_i^1, v_i^2, v_i^3, v_i^4, v_i^5, v_i^6, v_i^7, v_i^8, v_i^9, v_i^{10}, v_i^{11}, v_i^{12}, v_i^{13}), & \text{for } i = 1, 5, 7, 9; \\
 & (v_i^0, v_i^3, v_i^6, v_i^9, v_i^{12}, v_i^1, v_i^4, v_i^7, v_i^{10}, v_i^{13}, v_i^2, v_i^5, v_i^8, v_i^{11}), & \text{for } i = 2, 3, 4; \\
 & (v_i^0, v_i^5, v_i^{10}, v_i^1, v_i^6, v_i^{11}, v_i^2, v_i^7, v_i^{12}, v_i^3, v_i^8, v_i^{13}, v_i^4, v_i^9), & \text{for } i = 6, 8, 10.
 \end{aligned} \tag{7}$$

Theorem 29. *There exists an egc $4^3 0^2$ -graph Γ of order $140 \times k$ for every $0 < k \in \mathbb{Z}$ representing all color-cycle permutations, $14k$ times each.*

Proof. We assert that an egc $4^3 0^2$ -graph as in the statement contains $14k$ disjoint copies of Pet . We consider the case represented in the top of Fig. 14 for $k = 1$ and leave the details of the general case to the reader. Notice the 6-cycle $(v_5^j, v_6^j, v_7^j, v_8^j, v_9^j, v_{10}^j)$ in Pet^j with its three pairs of opposite vertices $\{v_5^j, v_8^j\}$ $\{v_6^j, v_9^j\}$ $\{v_7^j, v_{10}^j\}$ joined respectively to the neighbors v_2^j, v_3^j, v_4^j of the top vertex v_1^j for $j \in \mathbb{Z}_{14}$. A representation of the common proper coloring of the graphs Pet^j is in the lower-left part of Fig. 14, where the vertices v_i^j for $i = 1, \dots, 10$ and $j \in \mathbb{Z}_{14}$ are simply denoted i . This figure shows the twelve 5-cycles of Pet as color cycles, with red, black, blue, hazel and green taken respectively as 1, 2, 3, 4 and 5. This gives the one-to-one correspondence, call it η from the 5-cycles of Pet onto their color 5-cycles in the top part of Table 8.

There are exactly twelve color 5-cycles; they are the targets η . They are obtained from the $5! = 120$ permutations on five objects as the twelve orbits of the dihedral group D_{10} generated both by translations (mod 5) and by reflections of the 5-tuples on $\{1, 2, 3, 4, 5\}$. The edges of Γ not in $\cup_{j=0}^{13} \text{Pet}^j$ occur between different copies Pet^j of Pet ; these are colored as shown in the bottom part of Table 8. This insures the statement for $k = 1$ since the twelve vertical copies Pet^j of Pet are the only source of the color cycles. The extension of this for any $0 < k \in \mathbb{Z}$ is immediate. \square

The dodecahedral graph Dod with vertex set $\{u_i, w_i | i = 1, 2, \dots, 10\}$ and edge set formed by an edge pair $\{(u_i, w_{i'}), (u_{i'}, w_i)\}$ for each $(v_i, v_{i'}) \in (E(\text{Pet}) \setminus \{(v_5, v_6), (v_7, v_8), (v_9, v_{10})\})$ and an edge pair $\{(u_i, u_{i+1}), (w_i, w_{i+1})\}$ for each $i \in \{5, 7, 9\}$ is represented in the lower-right of Fig. 14, where u_i and w_i (that we will refer to as antipodal vertices) are respectively indicated by i and i' for $i = 1, \dots, 10$. Dod is a 2-covering graph of Pet via the graph map $\phi : \text{Dod} \rightarrow \text{Pet}$ such that $\phi^{-1}(\{v_i\}) = \{u_i, w_i\}$.

Theorem 30. *There exists an egc $2^3 0^2$ -graph Γ of order $140 \times k$ for every $0 < k \in \mathbb{Z}$.*

Proof. We consider the case $k = 1$ and leave the details of the general case to the reader. We take seven vertical copies of Dod presented in parallel at equal distances from left to right and numbered from 0 to 6 in \mathbb{Z}_7 . The vertices of the j -th copy Dod^j of Dod are denoted u_i^j and w_i^j for $i = 1, \dots, 10$ and are joined by the additional cycles

$$\begin{aligned} & (u_i^0, u_i^1, u_i^2, u_i^3, u_i^4, u_i^5, u_i^6, w_i^0, w_i^1, w_i^2, w_i^3, w_i^4, w_i^5, w_i^6), & \text{for } i = 1, 5, 7, 9; \\ & (u_i^0, u_i^3, u_i^6, u_i^2, u_i^5, u_i^1, u_i^4, w_i^0, w_i^3, w_i^6, w_i^2, w_i^5, w_i^1, w_i^4), & \text{for } i = 6, 8, 10; \\ & (u_i^0, u_i^5, u_i^3, u_i^1, u_i^6, u_i^4, u_i^2, w_i^0, w_i^5, w_i^3, w_i^1, w_i^6, w_i^4, w_i^2), & \text{for } i = 2, 3, 4. \end{aligned} \tag{8}$$

so that each such additional cycle passes through two antipodal vertices of each copy Dod^j . Notice the change of the order of the indices $i \in \{1, \dots, 10\}$ in the assignment of the additional cycles in display (8) with respect to the one in display (7). This is done to avoid the formation of 5-cycles not entirely contained in the copies Dod^j ($j \in \mathbb{Z}_7$). Since Dod has girth 5 and signature $2^3 = 222$ the graph Γ given by the union of the seven copies Dod^j and the just presented additional cycles is a $2^3 0^2$ -graph. By coloring the edges of the additional cycles of Γ via the same color pattern as in Theorem 29, it is seen that Γ is egc. \square

The truncated-icosahedral graph TI is the graph of the truncated icosahedron. This is obtained from the icosahedral graph, i.e. the line graph $\text{Ico} = L(\text{Dod})$ of Dod by replacing

(1, 2, 5, 10, 4) → (1, 2, 3, 4, 5)	(3, 6, 7, 8, 9) → (4, 1, 3, 5, 2)
(4, 1, 2, 8, 7) → (5, 1, 4, 3, 2)	(10, 9, 3, 6, 5) → (1, 2, 4, 5, 3)
(1, 2, 5, 6, 3) → (1, 2, 5, 4, 3)	(4, 7, 8, 9, 10) → (2, 3, 5, 1, 4)
(2, 5, 10, 9, 8) → (2, 3, 1, 5, 4)	(1, 3, 6, 7, 4) → (3, 4, 1, 2, 5)
(5, 10, 4, 7, 6) → (3, 4, 2, 1, 5)	(2, 8, 9, 3, 1) → (4, 5, 2, 3, 1)
(10, 4, 1, 3, 9) → (4, 5, 3, 2, 1)	(5, 6, 7, 8, 2) → (5, 1, 3, 4, 2)

(v_1^j, v_1^{j+1}) has color 2, if $j \equiv 0 \pmod{2}$ and 4, if $j \equiv 1 \pmod{2}$
(v_5^j, v_5^{j+1}) has color 1, if $j \equiv 0 \pmod{2}$ and 3, if $j \equiv 1 \pmod{2}$
(v_7^j, v_7^{j+1}) has color 5, if $j \equiv 0 \pmod{2}$ and 4, if $j \equiv 1 \pmod{2}$
(v_9^j, v_9^{j+1}) has color 3, if $j \equiv 0 \pmod{2}$ and 4, if $j \equiv 1 \pmod{2}$
(v_2^j, v_2^{j+3}) has color 5, if $j \equiv 0 \pmod{2}$ and 3, if $j \equiv 1 \pmod{2}$
(v_3^j, v_3^{j+3}) has color 1, if $j \equiv 0 \pmod{2}$ and 5, if $j \equiv 1 \pmod{2}$
(v_4^j, v_4^{j+3}) has color 1, if $j \equiv 0 \pmod{2}$ and 3, if $j \equiv 1 \pmod{2}$
(v_6^j, v_6^{j+5}) has color 3, if $j \equiv 0 \pmod{2}$ and 2, if $j \equiv 1 \pmod{2}$
(v_8^j, v_8^{j+5}) has color 1, if $j \equiv 0 \pmod{2}$ and 2, if $j \equiv 1 \pmod{2}$
(v_{10}^j, v_{10}^{j+5}) has color 5, if $j \equiv 0 \pmod{2}$ and 2, if $j \equiv 1 \pmod{2}$

Table 8: Color assignment of the $4^3 0^2$ -graph Γ in Theorem 29

each vertex v of Ico by a copy $C_5^{TI}(v)$ of its open neighborhood $N_{Ico}(v)$ considering all such copies $C_5^{TI}(v)$ pairwise disjoint, and replacing each edge (u, v) of Ico by an edge from the vertex corresponding to u in $C_5^{TI}(v)$ to the vertex corresponding to v in $C_5^{TI}(u)$. Note TI has sixty vertices, ninety edges, twelve 5-cycles, twenty 6-cycles and signature $1^2 0 = 110$.

Theorem 31. *There exists an egc 10^4 -graph on $840k$ vertices, for each integer $k > 0$.*

Proof. By means of a barrel-type construction as in Fig. 14, one can combine $14k$ copies of TI and the Cayley graph of \mathbb{Z}_{14} with generator set $\{1, 3, 5\}$ to get an egc graph as claimed. \square

Remark 32. The point graph of the generalized hexagon $GH(1, 5)$ [4, p. 204], the point graph of the Van Lint–Schrijver partial geometry [4, p. 307] and the odd graph [4, p. 259] on eleven points are distance-regular with intersection arrays $\{6, 5, 5; 1, 1, 6\}$, $\{6, 5, 5, 4; 1, 1, 2, 6\}$ and $\{6, 5, 5, 4, 4; 1, 1, 2, 2, 3\}$ respectively. If their chromatic number were 6, they would be $(125)^6$ -, $(25)^6$ - and $(25)^6$ -graphs, respectively, but it is known that none of them is egc.

7 Hamilton cycles and hamiltonian decomposability

Some feasible applications of egc graphs occur when the unions of pairs of composing 1-factors are Hamilton cycles, possibly attaining hamiltonian decomposability in the even-degree case. This offers a potential benefit to the applications drawn in Section 1, if an optimization/decision-making problem requires alternate inspections covering all nodes of the involved system, when the alternacy of two colors is required.

In Fig. 1, the cases (h–j) and their triangle-replaced graphs (m–o) as well as the case (u), and the 3-colored dodecahedral graph Dod that has the case (u) as its triangle replaced graph, have the unions of any two of their 1-factors forming a Hamilton cycle, while the cases (k), (p) and (v) have those unions as disjoint pairs of two cycles of equal length. In particular, the 3-cube graph Q_3 that admits just two tight factorizations, has one of them creating Hamilton cycle (case (l) via green and either red or blue edges, but not red and blue edges). The triangle-replaced graph, $\nabla(Q_3)$ has corresponding tight factorizations in cases (p–q) with similar differing properties as those of cases (k–l). Preceding Theorem 4, similar comments are made for $\nabla(\Gamma')$ where Γ' is Dod or the Coxeter graph Cox . Recall the union of two 1-factors of Dod is hamiltonian while the union of two 1-factors of Cox is not.

$s = 1$	5	7	9	11	13	15	$s = 3$	5	7	9	$s = 5$	5	7	9
$r = 6$	113						$r = 6$	131						
$r = 8$	211	114					$r = 8$	114	211					
$r = 10$	111	111	511				$r = 10$	111	511	111	$r = 10$	555	151	151
$r = 12$	213	312	112	116			$r = 12$	132	233	336	$r = 12$	611	611	211
$r = 14$	111	111	111	111	117		$r = 14$	141	111	111	$r = 14$	711	111	117
$r = 16$	211	114	114	112	211	118	$r = 16$	411	112	112	$r = 16$	811	211	211
$r = 18$	113	311	111	311	311	111	$r = 18$	131	131	333	$r = 18$	911	111	111
$r = 20$	211	112	215	215	112	112	$r = 20$	211	512	112	$r = 20$	$a51$	251	251
$r = 22$	111	111	111	111	111	111	$r = 22$	111	111	111	$r = 22$	$b11$	111	111
$r = 24$	213	314	411	611	611	114	$r = 24$	133	231	336	$r = 24$	$c11$	211	211
$r = 26$	111	111	111	111	111	111	$r = 26$	111	111	111	$r = 26$	$d11$	111	111
$r = 28$	211	112	211	211	217	711	$r = 28$	112	211	112	$r = 28$	$e11$	211	217
$r = 30$	113	311	115	115	111	111	$r = 30$	132	135	333	$r = 30$	$f11$	151	111

Table 9: Various cases of Theorem 10 item 3(e).

In Fig. 2(d), the three color partitions of Q_4 namely (12)(34), (13)(24) and (14)(23), yield 2-factorizations with 2-factors formed each by two cycles of equal length $\frac{1}{2}|V(Q_4)| = 8$. We denote this fact by writing $Q_4(2, 2, 2)$. In a likewise fashion, we can denote toroidal items in Fig. 2 as follows: (e) $\{4, 4\}_{12,2}^4(1, 4, 3)$ formed by 2-factorizations with 2-factors of one, three and four cycles of equal lengths 24, 6 and 8, respectively. Similarly: (f) $\{4, 4\}_{10,2}^4(1, 2, 1)$; (g) $\{4, 4\}_{6,3}^3(3, 3, 3)$; (h) $\{4, 4\}_{20,1}^0(2, 1, 1)$; (i) $\{4, 4\}_{28,1}^0(1, 1, 2)$; and (j) $\{4, 4\}_{22,1}^5(1, 2, 1)$.

Table 9 lists various cases of Theorem 10 item 3(e), indicating without parentheses or commas the triples abc corresponding to the numbers a b and c of cycles (of equal length in each case) of the respective 2-factors (12) (13) and (14).

Remark 33. For the toroidal cases in Theorem 10 item 3 depicted as in Fig. 2(f,g,h,j), assume that the 2-factors (12) and (14) complete 2-factorizations composed by 1-zigzagging cycles of equal length (i.e., composed by alternating horizontal and vertical edges) and that the 2-factors (13) and (24) are composed by vertical and horizontal edges, respectively. This way, while vertical edges form $\gcd(r, s)$ cycles of equal length, horizontal edges form t cycles

of not necessarily the same length, so the notation in the previous paragraph cannot be carried out for example for item 3(e) because $\gcd(r, s) \neq t$. So we modify that notation for such cases by simply writing $\{4, 4\}_{r,t}^s(a, b, c)$ that we call the *star notation* [12].

Theorem 34. *In the star notation of Remark 33, each applicable toroidal case $\Gamma = \{4, 4\}_{r,t}^s$ as in Theorem 10 is expressible as: $\{4, 4\}_{r,t}^s(\frac{1}{2} \gcd(r, |t - s|), \gcd(r, s), \frac{1}{2} \gcd(r, t + s))$.*

Proof. We prove the statement for the toroidal cases of Theorem 10 with two colors on horizontal cycles and the other two on vertical cycles, for the factorization $\{F_{12}, F_{34}\}$ and leave the rest to the reader. Consider the straight upper-right-to-lower-left line L_1 from the upper-right vertex $(0, 0)$ in the cutout Φ (Remark 5) of $\mathbb{Z}_r \times \mathbb{Z}_t$ passing through $(0, r - t + s)$ in the lower border of Φ and formed by the diagonals of $\frac{rt}{2\gcd(r, |t-s|)}$ squares representing 4-cycles of Γ . L_1 determines two 1-zigzagging cycles C_1^0, C_1^1 through $(0, 0)$ in F_{12}, F_{34} respectively, touching L_1 on alternate vertices of Γ . In the end, we get parallel lines L_1, \dots, L_z where $z = \frac{1}{2} \gcd(r, |t - s|)$ such that each L_i ($i = 1, \dots, z$) determines two 1-zigzagging cycles C_i^0, C_i^1 in F_{12}, F_{34} respectively, touching L_i at alternate vertices of Γ . An example is shown in Fig. 2(c) for $r = 12, t = 5, s = 9$ with $z = 2$ where L_1 is given in black thin trace and L_2 is given in gray thin trace, (not considering here the intermittent diagonals). \square

Corollary 35. *If $\frac{1}{2} \gcd(r, |t - s|) = \gcd(r, s) = \frac{1}{2} \gcd(r, t + s) = 1$ then the 2-factors (12) (34) (13) (14) and (23) are composed by a Hamilton cycle each (a total of six Hamilton cycles), comprising the 2-factorizations (12)(34) and (14)(23).*

Proof. This is due to Remark 33 and to the quadruple equality in the statement. \square

Additional examples are provided in display (9) for fixed $t = 2$ as in Theorem 10 item 3(b). The reader is invited to do similarly for Theorem 10, items 3(a) and 3(c).

r	$s = 4$	$s = 6$	r	$s = 4$	$s = 6$	r	$s = 4$	$s = 6$
8	141		14	121	121	20	141	122
10	121		16	141	124	22	121	121
12	143	162	18	123	131	24	143	164

(9)

Corollary 36. *In all cases of Theorem 10 item 2(b), there are exactly two hamiltonian 2-factorizations. Moreover, the toroidal graphs Γ in Theorem 10 are*

1. $\Gamma(222)$ for items 1(c)–2(a);
2. $\Gamma(211)$ for item 2(b) just for $s \equiv 1 \pmod{4}$;
3. $\Gamma(112)$ for item 2(b) just for $s \equiv 3 \pmod{4}$.

Proof. The toroidal graphs in Theorem 10 items 1(c) and 2(b) behave differently from those in Theorem 34 in that the 2-factors in question are 1-zigzagging in only one of the three 2-factorizations, while the other two 1-factorizations are 2-zigzagging, namely:

- (a) in Theorem 10 items 1(c) and 2(b), just for $s \equiv 1 \pmod{4}$ the 1-factorization (12)(34) is 1-zigzagging and the 1-factorizations (13)(24) and (14)(23) are 2-zigzagging;
- (b) in Theorem 10 item 2(b) just for $s \equiv 3 \pmod{4}$ the 2-factorizations (12)(34)–(13)(24) are 2-zigzagging and the 2-factorization (14)(23) is 1-zigzagging.

□

8 Applications to 3-dimensional geometry

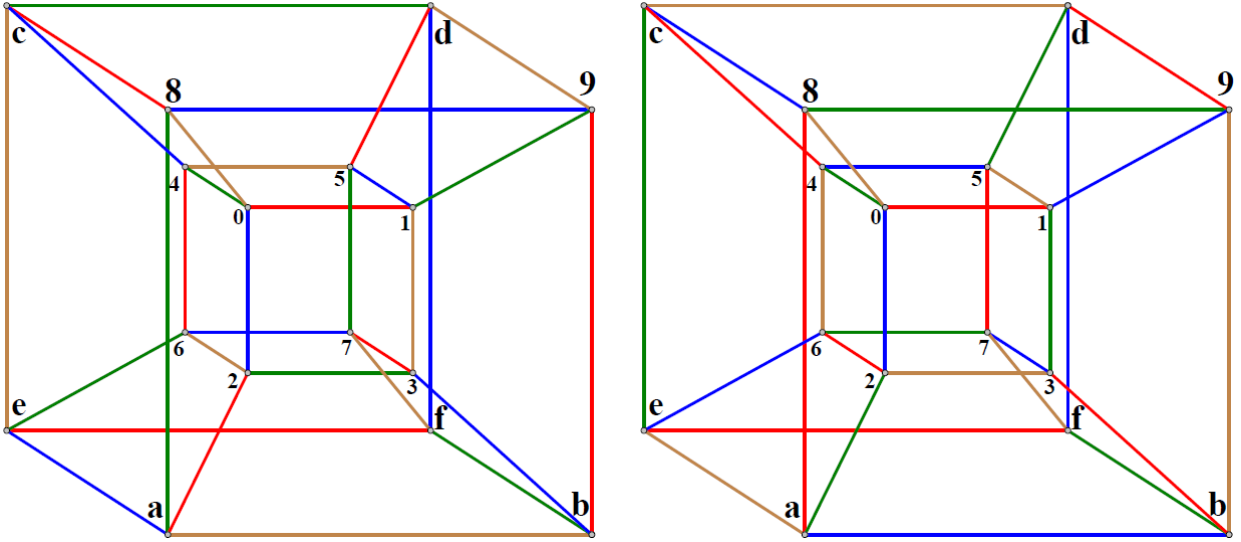


Figure 15: Two egc edge-colored 4-cube graphs.

Fig. 15 redraws the two toroidal copies of Q_4 in the lower center and right of Fig. 3 (arising in Subsection 3.1 from the central and right latin squares, respectively, in display (3)) as edge-colored 4-cubes with common vertex set $\{0, \dots, 7\} \cup \{i+8 = i' | i = 0, \dots, 7\}$ expressed in lowercase hexadecimal notation, in order to extract in Subsections 8.1, 8.2 and 8.3 piecewise linear (PL) (as in [26]) realizations of two enantiomorphic (i.e., mirror images of each other) compounds of four Möbius strips (as in [14, 16]). In the sequel, such pair of compounds is shown in Subsection 8.5 to be equivalent to corresponding enantiomorphic Holden-Odom-Coxeter polylinks of four locked hollow equilateral triangles each [9, 17, 18], from a group-theoretical point of view, having determined the automorphism group of the compounds in Subsection 8.4.

8.1 Compound of four PL Möbius strips

Theorem 37. *There exists a pair of enantiomorphic piecewise linear Möbius strip embedded in the hollow cube $[0, 3]^3 \setminus [1, 2]^3 \subset \mathbb{R}^3$ with piecewise linear closed curves as their boundary formed by segments parallel to the coordinate directions whose endvertices are points of \mathbb{Z}^3 .*

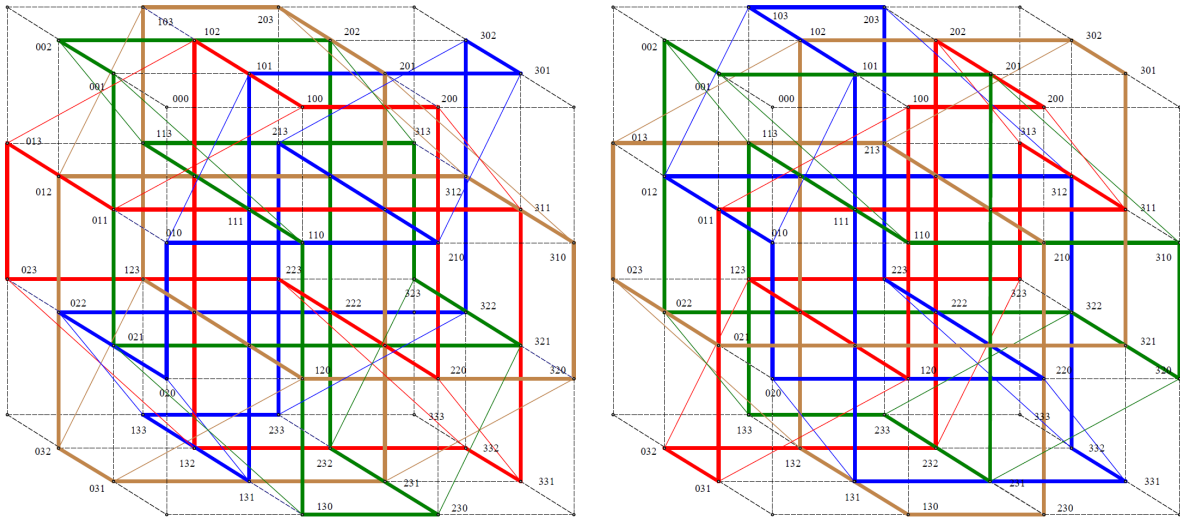


Figure 16: Two enantiomorphic quadruples of edge-disjoint PL knots 3_1 in $[0.3]^3$

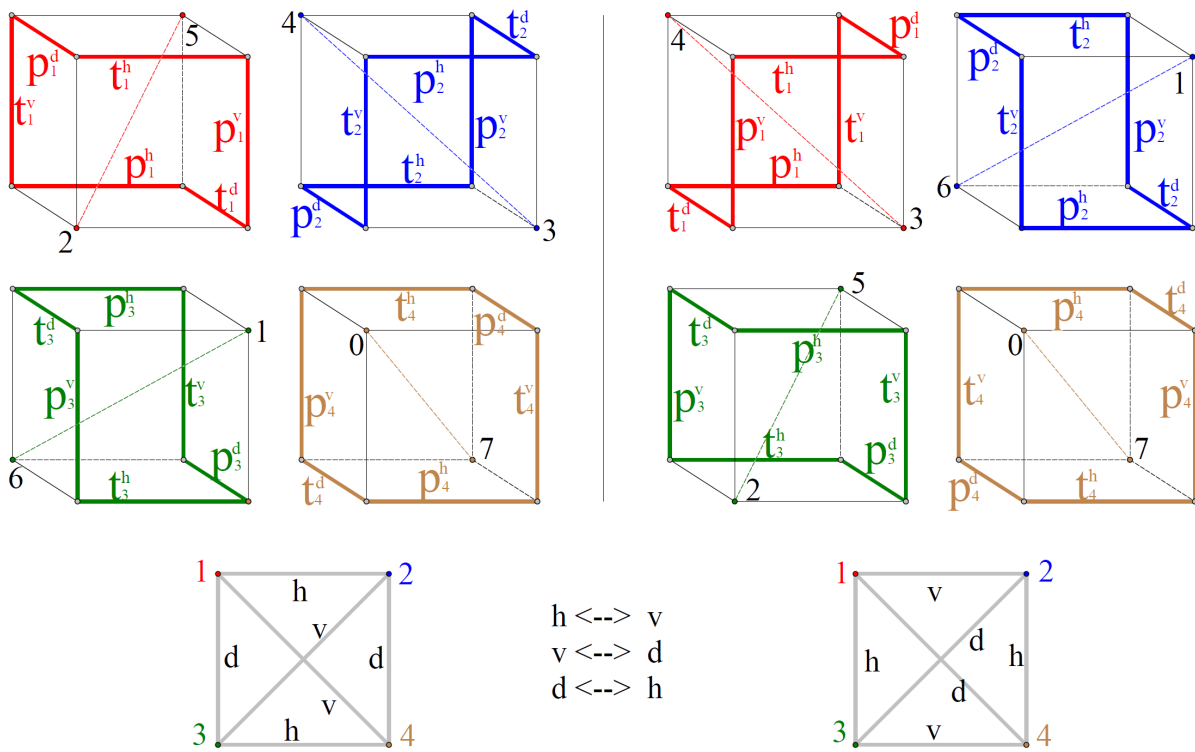


Figure 17: Edges of rotation.

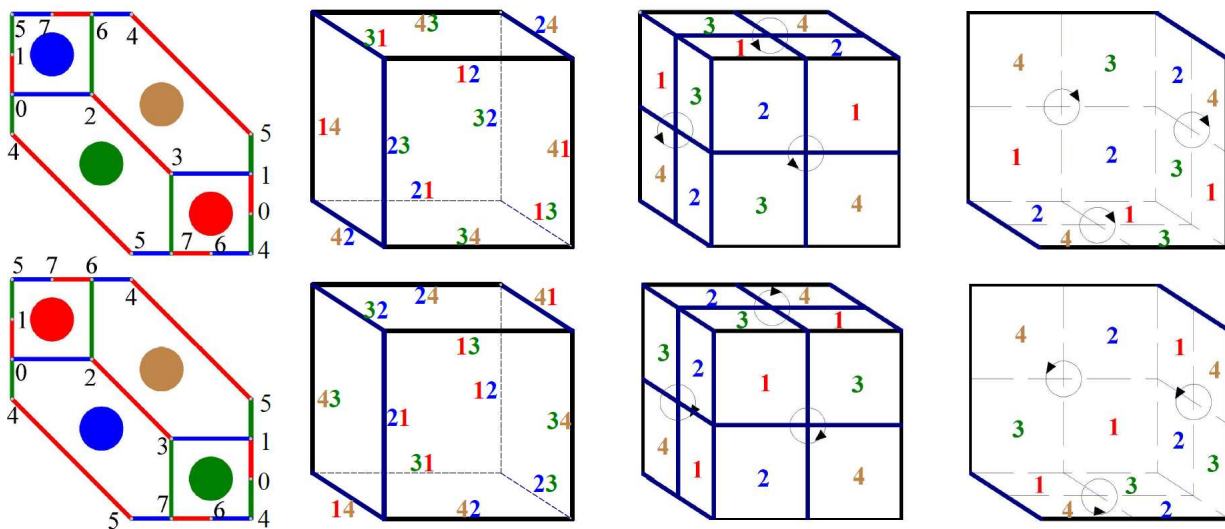


Figure 18: Assignment of pairs of colors to the edges of 3-cubes

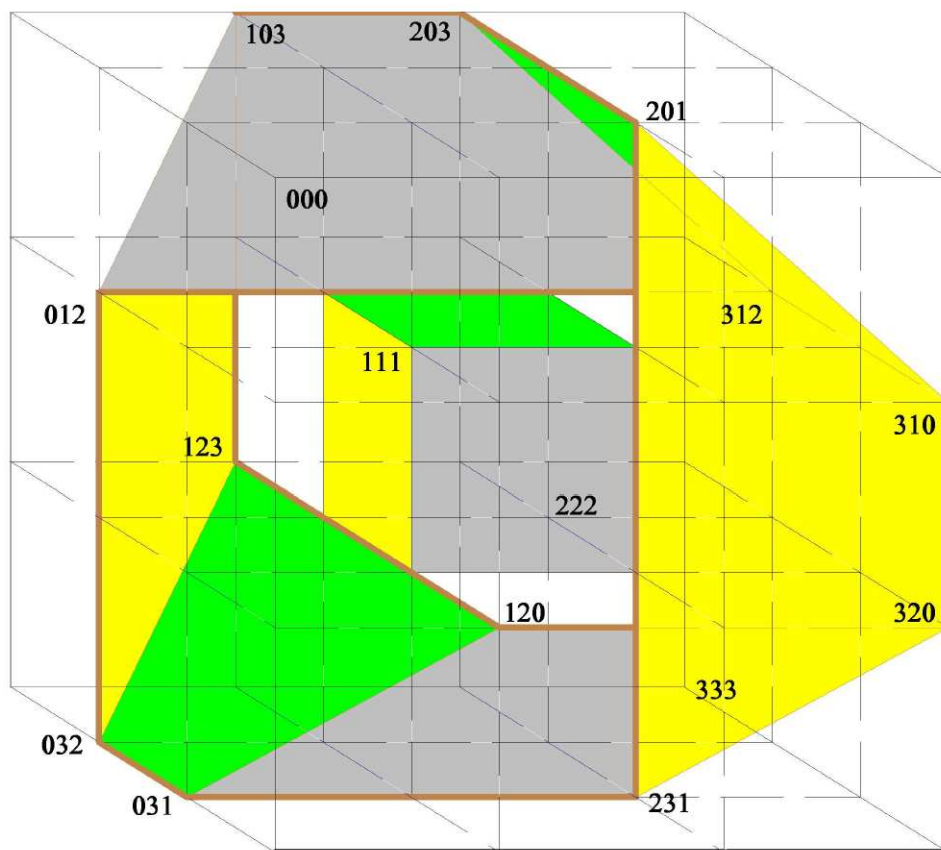


Figure 19: PL Möbius strip whose PL boundary has color 4 = hazel.

Proof. Fig. 16 represents two copies of the union $[0, 3]^3 \subset \mathbb{R}^3$ of 27 unit 3-cubes. In each such copy, Fig 16 highlights four disjoint *PL trefoil knots*, i.e. piecewise linear knots 3_1 [25, pp. 51–60] in thick trace (in contrast to the remaining edges of the 3-cubes, shown in dashed trace). Each such knot has its composing unit-length edges bearing a common color i , where $i = 1$ for red, $i = 2$ for blue, $i = 3$ for green and $i = 4$ for hazel. Accordingly, we denote C_i and C'_i for the PL trefoil knots in dark-traced color i in the left and right, respectively, of Fig. 16, for $i = 1, 2, 3, 4$. Note that $\cup_{i=1}^4 C'_i$ is an enantiomorph of $\cup_{i=1}^4 C_i$ and vice versa.

Each of the knots C_i or C'_i ($i = 1, 2, 3, 4$) is the boundary of a corresponding PL Möbius band M_i or M'_i , respectively, contained in the hollow cube $[0, 3]^3 \setminus [1, 2]^3$ formed by the 26 unit 3-cubes of $[0, 3]^3$ other than $[1, 2]^3$. In fact, each C_i or C'_i occurs in just 12 of the 26 unit cubes. Note that $\cup_{i=1}^4 M'_i$ is an enantiomorph of $\cup_{i=1}^4 M_i$ and vice versa.

Illustrated for M_i where $i = 4$, Fig. 19 exemplifies the fact that each M_i or M'_i is the union of six planar quadrilaterals, namely three (tilted) parallelograms and three (isosceles) trapezoids, in alternating contiguity, for $i = 1, 2, 3, 4$. In Fig. 19, colors gray, green and yellow highlight the visible parts of the planar faces of M_4 and of the central cube $[1, 2]^3$.

Still in Fig. 16, the sides of the six planar quadrilaterals of each M_i or M'_i ($i = 1, 2, 3, 4$) not in its boundary C_i or C'_i are in color- i thin trace so as to help visualize the parallelograms and trapezoids.

More specifically, the i -colored edges of the unit 3-cubes of $[0, 3]^3$ (illustrated in Fig. 19 for $i = 4$) form two parallel sides in each of the six quadrilaterals (with the occult parts in Fig. 19 in dashed trace, though visible on the left of Fig. 16). In the case of a trapezoid (resp., parallelogram) the lengths of those sides are 3 units internally and 1 unit externally (resp., 2 units internally and 2 units externally).

The sides of the hazel PL trefoil knot C_4 in Fig. 19 have their endvertex coordinates detailed in display (10), with colors of quadrilaterals cited between brackets starting clockwise at the left upper corner in Fig. 19, whether they are shown in full or in part, as indicated). In display (10), a segment denoted $[a_1 a_2 a_3, b_1 b_2 b_3]$ stands for $[(a_1, a_2, a_3), (b_1, b_2, b_3)]$, with $a_i, b_i \in \{0, 1, 2, 3\}$, ($i = 1, 2, 3$); each of the twelve segment brackets is appended with its length as a subindex and an element of $\{h, v, d\}$ as a superindex, where h, v , and d stand for horizontal, vertical and in-depth directions, respectively. The PL boundary curve C_4 is the hazel-colored PL trefoil knot in Fig. 19.

<i>gray(part)</i>	<i>green(part)</i>	<i>yellow(full)</i>	<i>gray(part)</i>	<i>green(full)</i>	<i>yellow(part)</i>	(10)
$[103, 203]_1^h$	$[203, 201]_2^v$	$[201, 231]_3^d$	$[231, 031]_2^h$	$[031, 032]_1^v$	$[032, 012]_2^d$	
$[012, 312]_3^h$	$[312, 310]_2^v$	$[310, 320]_1^d$	$[320, 120]_2^h$	$[120, 123]_3^v$	$[123, 103]_2^d$	

A similar display can be obtained for the other PL-trefoil knots, shown for C_2, C_3, C_4 respectively in displays (11), (12), (13), below. \square

Theorem 38. *There are four Möbius strips M_i in $[0, 3]^3 \setminus [1, 2]^3$ ($i = 1, 2, 3, 4$) with PL closed curves C_i as their corresponding boundaries; these are formed by segments parallel to the coordinate directions with endpoints in \mathbb{Z}^3 ; in fact, they are PL knots 3_1 with intersections in \mathbb{Z}^3 . Moreover, the compound $M = \cup_{i=1}^4 M_i$ has an enantiomorphic compound $M' = \cup_{i=1}^4 M'_i$ in $[0, 3]^3 \setminus [1, 2]^3$, formed by other four Möbius strips M'_i with similar properties to those of the M_i .*

Proof. To prove the statement, consider again the left of Fig. 16, where the hazel C_4 is drawn (and summarized in display (10)), as well as the red PL trefoil knot C_1 (bounding Möbius strip M_1), formed by the segments

$$\begin{array}{cccccc} [100, 200]_1^h & [200, 220]_v^2 & [220, 223]_3^d & [223, 023]_2^h & [023, 013]_1^v & [013, 011]_2^d \\ [011, 311]_3^h & [311, 331]_v^2 & [331, 332]_1^d & [332, 331]_2^h & [331, 102]_3^v & [102, 100]_2^d \end{array} \quad (11)$$

and the blue PL trefoil knot C_2 (bounding Möbius strip M_2), formed by the segments

$$\begin{array}{cccccc} [133, 233]_1^h & [233, 213]_2^v & [213, 210]_3^d & [210, 010]_2^h & [010, 020]_1^v & [020, 022]_2^d \\ [022, 322]_3^h & [322, 302]_2^v & [302, 301]_1^d & [301, 101]_2^h & [101, 131]_3^v & [131, 133]_2^d \end{array} \quad (12)$$

and the green PL trefoil knot C_3 (bounding Möbius strip M_3), formed by the segments

$$\begin{array}{cccccc} [230, 130]_1^h & [130, 110]_2^v & [110, 113]_3^d & [113, 313]_2^h & [313, 323]_1^v & [323, 321]_2^d \\ [321, 021]_3^h & [021, 001]_2^v & [001, 002]_1^d & [002, 202]_2^h & [202, 232]_3^v & [232, 230]_2^d \end{array} \quad (13)$$

The six planar faces of M_4 intersect C_4 in six corresponding pairs of segments, shown in display (10) vertically: first $[103, 203]_1^h$ above and $[012, 312]_3^h$ below, which delimit an isosceles trapezoid with the segments $[103, 012]$ and $[203, 312]$; then, $[203, 201]_2^v$ above, and $[312, 310]_2^v$ below, which delimit a parallelogram with the segments $[203, 312]$ and $[201, 310]$, etc. Similar observations can be made with respect to displays (11), (12) and (13). Similar conclusions can be obtained for C'_i ($i = 1, 2, 3, 4$). \square

8.2 Use of double egc girth-4-regular 4-cube

We denote the planar faces in displays (10), (11), (12) and (13) by means of the symbols $t_i^h, p_i^d, t_i^v, p_i^h, t_i^d, p_i^v$, respectively, ($i \in \{1, 2, 3, 4\} = \{\text{red, blue, green, hazel}\}$), as in the four left 3-cubes in the schematic Fig. 17.

In fact, Fig. 17 contains two sets of four copies of Q_3 each, the two sets differentiated by a vertical separator line, the leftmost set having its four copies of Q_4 already mentioned in the precious paragraph. These two sets of four copies of Q_4 correspond bijectively to the two sets of four trefoil knots in the copies of $[0, 3]^3$ in Fig. 16 so that each copy of Q_3 bears the monochromatic color of a corresponding trefoil knot. Then, each such copy of Q_3 is denoted Q_3^i where $i \in \{1, 2, 3, 4\} = \{\text{red, blue, green, hazel}\}$ is its monochromatic color in Fig. 17, that corresponds bijectively to the monochromatic color i of its associated PL trefoil knot in Fig. 16. (Recall that Fig. 16 contains two copies of each Q_3^i with color $i = 1$ for red, $i = 2$ for blue, $i = 3$ for green and $i = 4$ for hazel).

Two 6-cycles ξ_i and ζ_i are highlighted in thick trace on the left and right representations of Q_3^i in Fig. 17, respectively. Each copy of Q_3^i in Fig. 17 has its 6-cycle ξ_i or ζ_i with its highlighted edges marked x_i^j , where

1. $x = t$ for a trapezoid and $x = p$ for a parallelogram (both cases being quadrilaterals that are the faces of PL Möbius strips as in Fig. 16),
2. $i \in \{1, 2, 3, 4\}$ for associated color and

3. $j \in \{h, v, d\}$ for edge direction (h for horizontal, v for vertical and d for in-depth).

Each difference set $Q_3^i \setminus \xi_i$ or $Q_3^i \setminus \zeta_i$ appears in Fig. 17 as a pair of antipodal vertices in its copy of Q_3^i joined by a color- i dashed axis.

Below the left and right sets of four copies of Q_3 in Fig. 17 there are two corresponding auxiliary copies of K_4 whose vertices 1,2,3 and 4 correspond to, and are colored with, the red, blue, green and hazel of such copies of Q_3 , and where the edges bear labels h for horizontal, v for vertical and d for in-depth to indicate the directions of the only two shared edges of each pair of ξ_i or ζ_i . Between the two copies of K_4 the correspondence of colors between the ξ_i and the ζ_i is indicated.

We will establish now two bijections from the sets of four copies of Q_3 in Fig. 17 (representing M, M' in Theorem 37) onto the 1-factorizations F_1, F_2 of Q_4 in Subsection 3.1 illustrated in Fig. 3 and Fig. 15, with the subgraphs of Q_4 induced by the vertex subsets $\{0, 1, \dots, 7\}$ and $\{8, 9, a, b, c, d, e, f\}$ referred as *inner* and *outer*, respectively, copies of Q_3 in Q_4 .

Theorem 39. *There exists a bijection η from the edges denoted t_i^j (resp., p_i^j) in the 6-cycles ξ_i to the edges with color i and direction j in the inner (resp., outer) copy of Q_3 in the copy of Q_4 colored according to the 1-factorization F_1 .*

Proof. Display (14) demonstrates in detail the claimed bijection η where the rows are headed by the symbols $0_t, 0_p, 3_t, 3_p, 5_t, 5_p, 6_t, 6_p$ (corresponding to the alternate vertices 0,3,5,6 of Q_3 with subindices $x = t$ and $x = p$ for trapezoids and parallelograms, respectively, in Fig. 19), followed by three symbols x_i^j associated to the corresponding edges of the 6-cycles of Q_3 . The rest of each row is headed by the vertices 0, 8, 3, b , 5, d , 6, e , alternatively in the inner and outer 3-cube of the left 4-cube of Fig. 15, each such vertex followed by three edges associated bijectively with the three symbols x_i^j to their left, where $(0, 8)$, $(3, b)$, $(5, d)$, $(6, e)$ are vertex pairs corresponding to vertices 0,3,5,6 of Q_3 , respectively, and each edge in the inner and outer 3-cubes of Q_4 has its color in $\{1, 2, 3, 4\}$ as a subindex.

0_t	t_1^h	t_2^v	t_3^d	0	$(0, 1)_1$	$(0, 2)_2$	$(0, 4)_3$	
0_p	p_1^d	p_2^h	p_3^v	8	$(8, c)_1$	$(8, 9)_2$	$(8, a)_3$	
3_t	t_1^d	t_3^h	t_4^v	3	$(3, 7)_1$	$(3, 2)_3$	$(3, 1)_4$	
3_p	p_1^v	p_3^d	p_4^h	b	$(b, 9)_1$	$(b, f)_3$	$(b, a)_4$	
5_t		t_2^d	t_3^v	t_4^h	5	$(5, 1)_2$	$(5, 7)_3$	$(5, 4)_4$
5_p		p_2^v	p_3^h	p_4^d	d	$(d, f)_2$	$(d, e)_3$	$(d, 9)_4$
6_t	t_1^v	t_2^h	t_4^d	6	$(6, 4)_1$	$(6, 7)_2$	$(6, 2)_4$	
6_p	p_1^h	p_2^d	p_4^v	e	$(e, f)_1$	$(e, a)_2$	$(e, c)_4$	

(14)

□

Theorem 40. *There exists a bijection η' from the edges denoted t_i^j (resp., p_i^j) in the 6-cycles ζ_i to the edges with color i and direction j in the inner (resp., outer) copy of Q_3 in the copy of Q_4 colored according to the 1-factorization F_2 .*

Proof. Similar to the proof of Theorem 39 but replacing η by η' and display (14) by display (15).

0_t	t_1^h	t_2^v	t_3^d		0	$(0, 1)_1$	$(0, 2)_2$	$(0, 4)_3$	
0_p	p_1^v	p_2^d	p_3^h		8	$(8, a)_1$	$(8, c)_2$	$(8, 9)_3$	
3_t		t_2^d	t_3^v	t_4^h	3		$(3, 7)_2$	$(3, 1)_3$	$(3, 2)_4$
3_p		p_2^h	p_3^d	p_4^v	b		$(b, a)_2$	$(b, f)_3$	$(b, 9)_4$
5_t	t_1^v	t_2^h		t_4^d	5	$(5, 7)_1$	$(5, 4)_2$		$(5, 1)_4$
5_p	p_1^d	p_2^v		p_4^h	d	$(d, 9)_1$	$(d, f)_2$		$(d, c)_4$
6_t	t_1^d		t_3^h	t_4^d	6	$(6, 2)_1$		$(6, 7)_3$	$(6, 4)_4$
6_p	p_1^h		p_2^d	p_4^v	e	$(e, f)_1$		$(e, c)_3$	$(e, a)_4$

(15)

□

Remark 41. While the bijection in display (14) corresponds to the compound of four Möbius strips $\cup_{i=1}^4 M_i$ constructed in Subsection 8.1, the bijection in (15) corresponds to its enantiomorphic compound $\cup_{i=1}^4 M'_i$.

8.3 Petrie polygons

Remark 42. The four 6-cycles ξ_i (resp., ζ_i) on the left (resp., right) of Fig. 17 are the Petrie polygons (see [8]) of the 3-cube Q_3 viewed as a $\{4, 3\}$ -map, namely the regular map $\{6, 3\}_{2,0}$ in [8, Fig. 5] representing an embedding of the graph Q_3 into the torus, which we have slightly modified on the left of Fig. 18 representing $\cup_{i=1}^4 \xi_i$ on top (resp., $\cup_{i=1}^4 \zeta_i$ on the bottom), where solid colored circles indicate which Petrie polygons of Fig. 17 are represented, and vertices are denoted via a single digit 0, 1, 2, 3, 4, 5, 6, 7 standing for vertex 000, 001, 010, 011, 100, 101, 110, 111, respectively, in Fig. 16 or 19. In these representations of $\cup_{i=1}^4 \xi_i$ and $\cup_{i=1}^4 \zeta_i$ the edges are colored according to the coordinate directions along which they run: 1 for red, 2 for blue, 3 for green and 4 for hazel. Observe that ξ_i and ζ_i share exactly two antipodal edges along direction i , for $i = 1, 2, 3$, while ξ_4 coincides with ζ_4 .

In the rest of Fig. 18, to the right of the representations of $\cup_{i=1}^4 \xi_i$ and $\cup_{i=1}^4 \zeta_i$ the two leftmost 3-cubes have each of their edges assigned a pair of colors in $\{1, 2, 3, 4\}$. The first (resp., second) color is obtained from the corresponding row of 3-cubes in Fig. 17 as the color i of the only edge t_i^j (resp., p_i^j) in that edge position among the four cases in the row, where color numbers in Italics are employed for $i = 4$ (hazel) and in Roman for $i \in \{1, 2, 3\}$, (to distinguish red, blue and green). This allows an assignment from the color set $\{1, 2, 3, 4\}$ onto the set of 24 face quadrants of the 3-cube, shown in the right-center and right of Fig. 18 in each of the two cases, $\cup_{i=1}^4 \xi_i$ and $\cup_{i=1}^4 \zeta_i$. The faces in these 3-cubes are given an orientation each. The color pairs in Fig. 17 can be recovered from the quadrant colors in Fig. 18 by reading them along an edge according to the corresponding face orientation.

Let us look at the segmental intersections of trapezoids and parallelograms in $M = M_1 \cup M_2 \cup M_3 \cup M_4$ from displays (10), (11), (12) and (13).

The top-front set $TF_i^h = ([000, 300] \times [000, 010] \times [000, 001]) \cap M_i$ of $[0, 3]^3$ in Fig. 16 is trapezoid t_1^h for $i = 1$ and parallelogram p_2^h for $i = 2$. In the upper leftmost cube in

Fig. 18, let us call it Q , we indicate the corresponding segmental intersection $t_1^h \cap t_2^h$ via the edge-labelling pair 12, with 1 in red and 2 in blue, namely the colors used to represent C_1 and C_2 , respectively. This pair 12 labels the top-front horizontal edge of Q , corresponding to the position of $TF_1^h \cap TF_2^h = t_1^h \cap p_2^h$ in Fig. 16.

In all edge-labelling pairs in Q (Fig. 18), the first number is associated to a trapezoid and the second one to a parallelogram, each number printed in its associated color.

We subdivide the six faces of Q into four quarters each, and label such quarters with the numbers 1 to 4, setting external counterclockwise (or internal clockwise) orientations to the faces, so that the two numbers corresponding to an edge of any given face yield, via the defined orientation, the labelling pair as defined above. This is represented in the upper center and upper right 3-cubes in Fig. 18.

We can identify the cube Q with the union of the pairwise distinct intersections $M_i \cap M_j$, ($1 \leq i < j \leq 4$). This union becomes formed by the segments:

$$\begin{aligned}
& [(0.5,0.5,0.5),(2.5,0.5,0.5)]_1^2 [(0.5,2.5,0.5),(2.5,2.5,0.5)]_2^4 [(0.5,0.5,2.5),(2.5,0.5,2.5)]_2^1 [(0.5,2.5,2.5),(2.5,2.5,2.5)]_4^2 \\
& [(0.5,0.5,0.5),(0.5,2.5,0.5)]_2^3 [(2.5,0.5,0.5),(2.5,2.5,0.5)]_3^4 [(0.5,0.5,2.5),(0.5,2.5,2.5)]_3^2 [(2.5,0.5,2.5),(2.5,2.5,2.5)]_4^3 \\
& [(0.5,0.5,0.5),(0.5,0.5,2.5)]_3^1 [(2.5,0.5,0.5),(2.5,0.5,2.5)]_1^4 [(0.5,2.5,0.5),(0.5,2.5,2.5)]_1^3 [(2.5,2.5,0.5),(2.5,2.5,2.5)]_4^1
\end{aligned} \tag{16}$$

where each segment has its trapezoid color number as a subindex and its parallelogram color number as a superindex. The first, second and third lines in (16) display those segments of Q parallel to the first, second and third coordinates, respectively.

8.4 Automorphism group of the compound

Theorem 43. *The automorphism group $G = \text{Aut}(M)$ of $M = \bigcup_{i=1}^4 M_i$ is isomorphic to the group of 24 rotations of the 3-cube, that is the symmetry group Sym_4 of four elements. Moreover, the 24 reflections of the cube takes M bijectively into an enantiomorph of M also obtainable from M' by rotations.*

Proof. The symmetries of M coincide with the 24 rotations of the 3-cube $[1, 2]^3$, namely the identity plus 9 rotations around the lines joining the centers of opposite faces plus 8 rotations around the lines joining opposite vertices plus 6 rotations around the lines joining the centers of opposite edge. On the other hand. the 24 reflections of M through the center $(1.5, 1.5, 1.5)$ of $[1, 2]^3$ takes M into na enantiomorph of M isomorphic to M' . \square

8.5 Polylink of four hollow triangles

A sculpture by G. P. Odom Jr., see Fig. 20, was analyzed by H. S. M. Coxeter [9], for its geometric and symmetric properties. According to [27, p. 270], Odom and Coxeter were unaware of the earlier discovery [17] of this by A. Holden, who called it a *regular polylink of four locked hollow triangles* [18].

We relate the top Möbius-strip compound above to this structure, noting that the centers of the maximum linear parts of the PL trefoil knots C_i ($i = 1, 2, 3, 4$) are the vertices of four

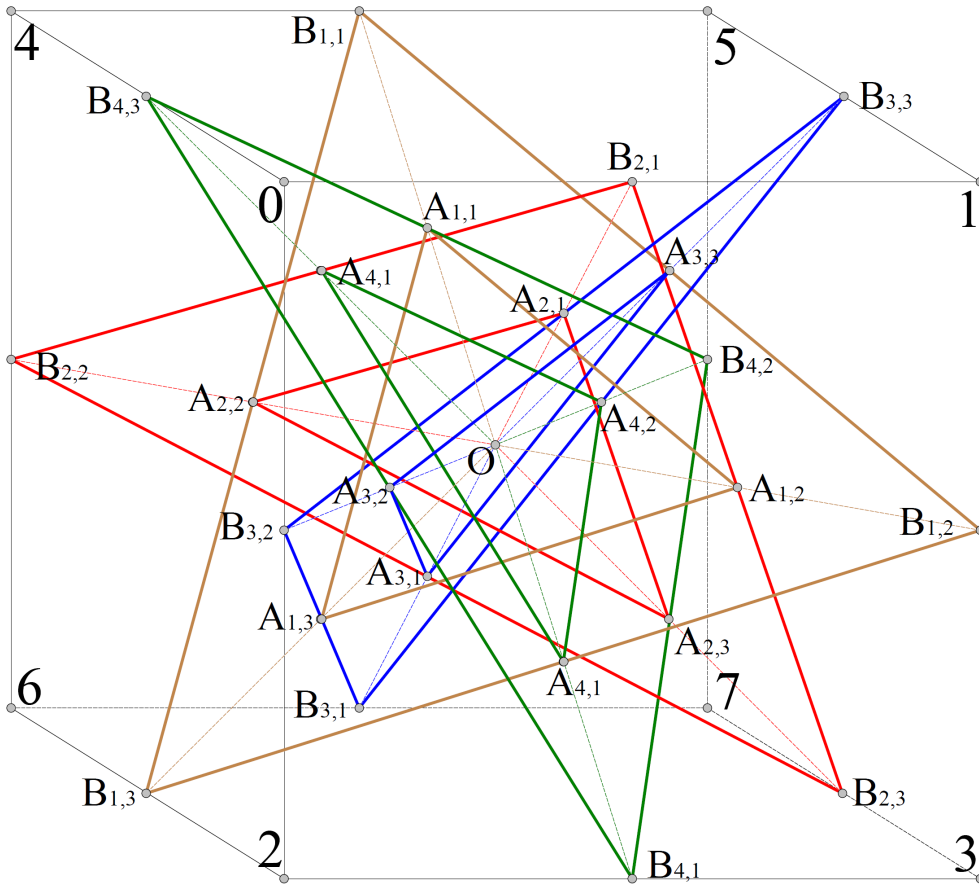


Figure 20: Odom-Coxeter polylink.

corresponding equilateral triangles, namely (in the order of the triangle colors):

$$\begin{array}{l} 1 \quad (1.5, 0, 3), \quad (3, 1.5, 0), \quad (0, 3, 1.5); \\ 3 : \quad (1.5, 3, 3), \quad (0, 1.5, 0), \quad (3, 0, 1.5); \end{array} \left| \begin{array}{l} 2 : \quad (1.5, 0, 0), \quad (0, 1.5, 3), \quad (3, 3, 1.5); \\ 4 : \quad (1.5, 3, 0), \quad (3, 1.5, 3), \quad (0, 0, 1.5). \end{array} \right. \quad (17)$$

Each of these triangles T_i ($i = 1, 2, 3, 4$), gives place to a hollow triangle (i.e., a planar region bounded by two homothetic and concentric equilateral triangles [9]) by removing from T_i the equilateral triangle T'_i whose vertices are the midpoints of the segments between the vertices of T_i (display (17)) and $O = (1.5, 1.5, 1.5)$. Characterized by colors, these midpoints are

$$\begin{array}{l} 1 : \quad (1.50, 0.75, 2.25), \quad (2, 25, 1.50, 0.75), \quad (0.75, 2.25, 1.50); \\ 2 : \quad (1.50, 0.75, 0.75), \quad (0.75, 1.50, 2.25), \quad (2.25, 2.25, 1.50); \\ 3 : \quad (1.50, 2.25, 2.25), \quad (0.75, 1.50, 0.75), \quad (2.25, 0.75, 1.50); \\ 4 : \quad (1.50, 2.25, 0.75), \quad (2.25, 1.50, 2.25), \quad (0.75, 0.75, 1.50). \end{array} \quad (18)$$

The centers in display (17) are the vertices of an Archimedean cuboctahedron. Consider the midpoints of the sides of the triangles T_i , namely:

$$\begin{array}{l} 1 : \quad (2.25, 0.75, 1.50), \quad (1.50, 2.25, 0.75), \quad (0.75, 1.50, 2.25); \\ 2 : \quad (0.75, 0.75, 1.50), \quad (1.50, 2.25, 2.25), \quad (2.25, 1.50, 0.75); \\ 3 : \quad (0.75, 2.25, 1.50), \quad (1.50, 0.75, 0.75), \quad (2.25, 1.50, 2.25); \\ 4 : \quad (2.25, 2.25, 1.50), \quad (1.50, 0.75, 2.25); \quad (0.75, 1.50, 0.75). \end{array} \quad (19)$$

By expressing the 3-tuples in (18) via a 4×3 -matrix $\{A_{i,j}; i = 1, 2, 3; j = 1, 2, 3, 4\}$, we have the following correspondence from (18) to (19), in terms of the notation in Fig. 20:

$$\begin{pmatrix} A_{1,1} & A_{1,2} & A_{1,3} \\ A_{2,1} & A_{2,2} & A_{2,3} \\ A_{3,1} & A_{3,2} & A_{3,3} \\ A_{4,1} & A_{4,2} & A_{4,3} \end{pmatrix} \rightarrow \begin{pmatrix} B_{1,12} & B_{1,23} & B_{1,31} \\ B_{2,12} & B_{2,23} & B_{2,31} \\ B_{3,12} & B_{3,23} & B_{3,31} \\ B_{4,12} & B_{4,23} & B_{4,31} \end{pmatrix} = \begin{pmatrix} A_{3,3} & A_{4,1} & A_{2,2} \\ A_{4,3} & A_{3,1} & A_{1,2} \\ A_{1,3} & A_{2,1} & A_{4,2} \\ A_{2,3} & A_{1,1} & A_{3,2} \end{pmatrix} \quad (20)$$

meaning each midpoint $B_{i,jk}$ of a T_i between $B_{i,j}$ and $B_{i,k}$ equals a vertex $A_{i',j'}$ of some $T_{i'}$, and vice-versa, as in Fig. 20. Take each T_i as the 6-cycle of its vertices and side midpoints:

$$\begin{array}{l} T_1 = \quad (B_{1,1} \quad A_{3,3} \quad B_{1,2} \quad A_{4,1} \quad B_{1,3} \quad A_{2,2}); \\ T_2 = \quad (B_{2,1} \quad A_{1,2} \quad B_{2,3} \quad A_{3,1} \quad B_{2,2} \quad A_{4,1}); \\ T_3 = \quad (B_{3,1} \quad A_{1,3} \quad B_{3,2} \quad A_{2,1} \quad B_{3,3} \quad A_{4,2}); \\ T_4 = \quad (B_{4,1} \quad A_{1,1} \quad B_{4,2} \quad A_{2,3} \quad B_{4,1} \quad A_{3,2}). \end{array} \quad (21)$$

Corollary 44. *The automorphism group of the union $\bigcup_{i=1}^4 T_i$ is $G = \text{Aut}(\bigcup_{i=1}^4 M_i) = \text{Aut}(\bigcup_{i=1}^4 T_i)$. In addition, $G_i = \text{Aut}(M_i) = \text{Aut}(T_i)$, for each $i = 1, 2, 3, 4$, is isomorphic to the dihedral group of six elements. Moreover, there are only two polylinks of four hollow triangles in $[0, 3]^3$, including $\bigcup_{i=1}^4 T_i$, and these two polylinks are enantiomorphic.*

Proof. By expressing, as in Fig. 20, the vertices of $[0, 3]^3$ by:

$$\mathbf{0} = 000, \quad \mathbf{1} = 300, \quad \mathbf{2} = 030, \quad \mathbf{3} = 330, \quad \mathbf{4} = 003, \quad \mathbf{5} = 303, \quad \mathbf{6} = 033, \quad \mathbf{7} = 033, \quad (22)$$

we notice that the $\pm 120^\circ$ angle rotations of $[0, 3]^3$ around the axis line determined by the two points of color i in Q , as indicated in Fig. 17, correspond respectively to the permutations:

$$\begin{aligned} \text{Color 1 : } R_1 &= (\mathbf{124})(\mathbf{365}) & \text{and} & \quad R_1^{-1} = (\mathbf{142})(\mathbf{563}); \\ \text{Color 2 : } R_2 &= (\mathbf{036})(\mathbf{174}) & \text{and} & \quad R_2^{-1} = (\mathbf{063})(\mathbf{147}); \\ \text{Color 3 : } R_3 &= (\mathbf{065})(\mathbf{271}) & \text{and} & \quad R_3^{-1} = (\mathbf{056})(\mathbf{217}); \\ \text{Color 4 : } R_4 &= (\mathbf{247})(\mathbf{053}) & \text{and} & \quad R_4^{-1} = (\mathbf{274})(\mathbf{035}), \end{aligned} \quad (23)$$

where color 1 is red, color 2 is blue, color 3 is green and color 4 is hazel; notice also that the axes in Q corresponding to these colors are:

$$\begin{aligned} &[(0.5, 0.5, 0.5), (2.5, 2.5, 2.5)], & & [(0.5, 2.5, 0.5), (2.5, 0.5, 2.5)], \\ &[(0.5, 0.5, 2.5), (2.5, 2.5, 0.5)], & & [(2.5, 0.5, 0.5), (0.5, 2.5, 2.5)]. \end{aligned}$$

The rest of the statement arises from Theorem 43. The fact that there are two polylinks of four hollow triangles in $[0, 3]^3$ that are enantiomorphic is inherited from Theorem 43. \square

References

- [1] S. Ali, M. K. Jamil, M. Azeem, M. A. Zahid, T. A. Ismail, *Double resolving sets and the exchange property with applications in network optimization and cybersecurity*, Materials Chemistry and Physics, (2025) DOI: 10.1016/j.matchemphys.2025.131289
- [2] M. Azeem, *Cycle-super magic labeling of polyomino linear and zig-zag chains*, Journal of Operations Intelligence, **1.1**.(2023): 67–81. <https://doi.org/10.31181/jopi1120235>.
- [3] C. Armanios, *A new 5-valent distance transitive graph*, Ars Combin. **19A** (1985), 77–85.
- [4] A. Brouwer, A. Neumaier, A. Cohen, *Distance-Regular Graphs*, Springer-Verlag, 1998.
- [5] C. J. Colbourn, J. H. Dinitz, *Handbook of Combinatorial Designs* (2nd ed.), Boca Raton: Chapman & Hall/ CRC, (2007).
- [6] J. H. Conway, N. J. A. Sloane, *Sphere Packings, Lattices and Groups*, (3rd ed.), Berlin, New York: Springer-Verlag, (1999).
- [7] S. L. R. Costa, R. Muniz, E. Agustini, R. Palazzo, *Graphs, Tessellations and Perfect Codes in Flat Tori*, IEEE Transactions on Information Theory, **50-10**(2004), 2363-2377.
- [8] H. S. M. Coxeter, *Self-dual configurations and regular graphs*, Bull. Amer. Math. Soc., **56(5)** (1950), 413–455.
- [9] H. S. M. Coxeter, *Symmetrical Combinations of Three or Four Hollow Triangles*, The Mathematical Intelligencer, **16(3)** (1994), 25–30.

- [10] H. S. M. Coxeter, *Self-Dual Configurations and Regular Graphs*, Bull. Amer. Math. Soc. **56** (1950), 413–455.
- [11] P. R. Cromwell, *Polyhedra*, Cambridge Univ. Press, Cambridge UK (1997).
- [12] I. J. Dejter, O. Serra, *Efficient dominating sets in Cayley graphs*, Discrete Applied Mathematics **129**(2–3) (2002), 319–328.
- [13] E. Eiben, R. Jajcay, P. Šparl, *Symmetry properties of generalized graph truncations*, J. Combin. Theory, Ser. B **137** (2019) 29–131.
- [14] D. Fuchs, S. Tabachnikov, *Mathematical Omnibus: Thirty Lectures on Classic Mathematics*, 2007, 199–206, at <http://www.math.psu.edu/tabachni/Books/taaba.pdf>
- [15] G. Haidar, S. Ali, W. Khan, *Fault-tolerant topological indices of graph joins with applications in multi-swarm drone networks*, Computer Networks, **270**(2025) DOI: 10.1016/j.comnet.2025.111517
- [16] D. Hilbert, S. Cohn-Vossen, *Geometry and the Imagination* (2nd ed.), Chelsea, 1952.
- [17] A. Holden, *Shapes, Spaces and Symmetry*, Columbia Univ. Press, 1971.
- [18] A. Holden, *Regular Polylinks*, Structural Topology, **4** (1980), 41–45.
- [19] W. Imrich, S. Klavžar, D. F. Rall, *Graphs and their cartesian products*, A. K. Peters, (2008).
- [20] A. Khan, S. Ali, S. Hayat, M. Azeem, Y. Zhong, M. A. Zahid, M. J.F. Alenazi, *Fault-tolerance and unique identification of vertices and edges in a graph: The fault-tolerant mixed metric dimension*, Journal of Parallel and Distributed Computing, **197** (2025), <https://doi.org/10.1016/j.jpdc.2024.105024>.
- [21] P. Potočnik, P. Spiga, G. Verret, *A census of cubic vertex-transitive graphs*
<https://staff.matapp.unimib.it/~spiga/census.html>.
- [22] P. Potočnik, J. Vidali, *Girth-regular graphs*, Ars Mathematica Contemporanea, **17** (2019), 349–368.
- [23] P. Potočnik, S. Wilson, *Tetravalent edge-transitive graphs of girth at most 4*, Jour. Combin. Theory, Ser. B, **97** (2007), 217–236.
- [24] P. Potočnik, S. Wilson, *Linking-ring structures and tetravalent semisymmetric graphs*, Ars. Math. Contemporanea, **7** (2014), 341–352.
- [25] D. Rolfsen, *Knots and Links*, Publish or Perish Press, Wilmington DE, 1976
- [26] C. P. Rourke, B. J. Sanderson, *Introduction to Piecewise-Linear Topology*, Springer, New York, NY, 1972.

- [27] D. Schattschneider, *Coxeter and the Artists: 2-Way Inspiration*, in *The Coxeter Legacy, Reflections and Projections*, (ed. C. Davis et al.), Amer. Math. Soc., 2006.
- [28] Y. Tu, S. Ali, M. Azeem, M. Arshad, G. Haidar, H. K. Thabet, *Optimizing emergency response services in urban areas through the fault-tolerant metric dimension of hexagonal nanosheet*, *Scientific Reports*, **15(1)** (2025) DOI:10.1038/s41598-025-16684-0.
- [29] W. D. Wallis, *One-Factorizations (Math. and its Appl.)*, Springer, NY, 1997.
- [30] S. Wilson, *Uniform maps on the Klein bottle*, *Jour. for Geom. and Graphics*, **10(2)** (2006), 161–171.
- [31] S. Wilson, P. Potočník, *Recipes for edge-transitive tetravalent graphs*, *Art Discrete Appl. Math.*, **3** (2020), 33 pp.
- [32] S. N. A. Zamri, S. Ali, M. Azeem, H. A. Neamah, B. Almohsen, *The Mixed Partition Dimension: A New Resolvability Parameter in Graph Theory*. *IEEE Access* (2025). DOI: 10.1109/ACCESS.2025.3534819.